JAMES | Journal of Advances in Modeling Earth Systems

RESEARCH ARTICLE
10.1029/2022MS003074

Implementation and Evaluation of Irrigation Techniques in the Community Land Model

Yi Yao[1], Inne Vanderkelen[1], Danica Lombardozzi[2], Sean Swenson[2], David Lawrence[2], Jonas Jägermeyr[3,4,5], Luke Grant[1], and Wim Thiery[1]

[1]Department of Hydrology and Hydraulic Engineering, Vrije Universiteit Brussel, Brussels, Belgium, [2]National Center for Atmospheric Research, Boulder, CO, USA, [3]Potsdam Institute for Climate Impact Research, Member of the Leibniz Association, Potsdam, Germany, [4]Department of Computer Science, University of Chicago, Chicago, IL, USA, [5]NASA Goddard Institute for Space Studies, New York, NY, USA

Key Points:

- A newly-developed irrigation module considering different irrigation methods is implemented in Community Land Model
- The new irrigation scheme shows a better performance of simulating irrigation water withdrawal against the original module
- Different irrigation methods have different effects on water cycle and energy budgets, changing regional irrigation-induced impacts

Correspondence to:
Y. Yao,
yi.yao@vub.be

Citation:
Yao, Y., Vanderkelen, I., Lombardozzi, D., Swenson, S., Lawrence, D., Jägermeyr, J., et al. (2022). Implementation and evaluation of irrigation techniques in the Community Land Model. *Journal of Advances in Modeling Earth Systems*, *14*, e2022MS003074. https://doi.org/10.1029/2022MS003074

Received 11 MAR 2022
Accepted 25 OCT 2022

Author Contributions:
Conceptualization: Yi Yao, Inne Vanderkelen, Danica Lombardozzi, Sean Swenson, David Lawrence, Jonas Jägermeyr, Wim Thiery
Data curation: Yi Yao, Inne Vanderkelen, Luke Grant
Formal analysis: Yi Yao
Funding acquisition: Wim Thiery
Investigation: Yi Yao, Inne Vanderkelen, Danica Lombardozzi, Sean Swenson, David Lawrence, Jonas Jägermeyr, Wim Thiery

Abstract Several previous studies have highlighted the irrigation-induced impacts on the global and regional water cycle, energy budget, and near-surface climate. While land models are widely used to address this question, the implementations of irrigation in these models vary in complexity. Here, we expand the representation of irrigation in Community Land Model to enable six different irrigation methods. We find that using a combination of irrigation methods, including default, sprinkler, flood and paddy techniques performs best as determined by evaluating the simulated irrigation water withdrawals against observations, and therefore select this combination as the new irrigation scheme. Then, the impact of the new irrigation scheme on surface fluxes is evaluated and detected using single-point simulations. Finally, the global and regional irrigation-induced impacts on surface energy and water fluxes are compared using both the original and the new irrigation scheme. The new irrigation scheme substantially reduces the bias and root-mean-square error of simulated irrigation water withdrawal in the USA and other countries, but considerably overestimates withdrawals in Central China. Results of single-point experiments show that different irrigation methods have different effects on surface fluxes, while the magnitudes are small. At the global scale, the new scheme enlarges the irrigation-induced impacts on water and energy variables relative to the original scheme, with varying magnitudes across regions. Overall, our results suggest that this newly developed scheme is a better tool for simulating irrigation-induced impacts on climate, and highlight the added value of incorporating human water management in Earth system models.

Plain Language Summary Knowing the effects of irrigation on the water and energy cycle is important, as it helps us to understand better how irrigation may affect the near-surface climate such as dampening heat extremes and increasing local air humidity. Land models are widely used for this purpose. However, in most of these models, different irrigation techniques are currently not considered. In this study, we develop a new irrigation scheme for the Community Land Model, and evaluate it by comparing modeled and observed irrigation water withdrawals and surface energy and water fluxes. Results show that this new scheme performs better in simulating irrigation water withdrawals in most countries. Results of one-dimensional simulations show that different irrigation methods have small but varying impacts on surface fluxes. At the global and regional scale, incorporating more realistic irrigation methods enlarges the effects of irrigation on water and energy variables. We therefore conclude that improving the realism of irrigation in models can help us to improve our understanding of how irrigation affects climate through altered water and energy fluxes.

1. Introduction

Irrigation is an important aspect of agricultural management, with irrigated areas providing ~40% of global food production over only ~20% of global cropland (WWAP, 2019). It is fundamental to the food security of less developed countries, where populations have experienced fast growth (Schultz et al., 2005). Since the 1950s, the global irrigated land area has expanded rapidly, thereby increasing worldwide irrigation water demand. Consequently, irrigation currently accounts for ~90% (~1,200 km^3 by the end of 20th century) of the global total consumptive freshwater use (Döll et al., 2009; Meier et al., 2018; Siebert et al., 2015; Zohaib & Choi, 2020).

As the most dominant freshwater-use practice, irrigation plays an important role in global and regional environmental change. Irrigation practices move water from different sources into agricultural systems, altering the global

Methodology: Yi Yao, Inne Vanderkelen, Danica Lombardozzi, Sean Swenson, David Lawrence, Jonas Jägermeyr, Wim Thiery
Resources: Danica Lombardozzi, Sean Swenson, David Lawrence, Wim Thiery
Software: Yi Yao, Inne Vanderkelen, Danica Lombardozzi, Sean Swenson
Supervision: Inne Vanderkelen, Danica Lombardozzi
Validation: Yi Yao
Visualization: Yi Yao, Inne Vanderkelen
Writing – original draft: Yi Yao
Writing – review & editing: Yi Yao, Inne Vanderkelen, Danica Lombardozzi, Sean Swenson, Jonas Jägermeyr, Luke Grant

and regional hydrological cycle (de Vrese et al., 2016; Ferguson & Maxwell, 2012; Harding & Snyder, 2012; Leng et al., 2014). In some regions, the extraction of water for irrigation has reduced the availability of both surface and groundwater. For example, the discharge of the Tarim River basin in northwestern China has decreased substantially since 1960s, as 70%–90% of surface water flows are used for irrigation (Hao et al., 2015). In the High Plains in the USA, the water level of aquifers has declined substantially due to the large irrigation water withdrawal (McGuire, 2014). A study focusing on global lakes revealed that ∼11% of the lake area has been lost until 2015 mainly due to irrigation water withdrawal (Wine & Laronne, 2020).

In addition to modifying water fluxes, irrigation also alters the surface energy balance and thereby near-surface climate. Most importantly, the increase of surface soil moisture results in higher evaporation (Puma & Cook, 2010), which drives lower sensible heat flux (SHF) over irrigated areas (Cook et al., 2015; Ferguson & Maxwell, 2012; Hauser et al., 2019; Hirsch et al., 2017; Thiery et al., 2017). In addition, irrigation-induced feedbacks can also alter downwelling shortwave radiation, downwelling longwave radiation, surface albedo, and net radiation (Rnet) (Cook et al., 2011; Thiery et al., 2017). These modified surface energy fluxes subsequently alter near-surface climate. For example, various observation-based and modeling studies have shown that irrigation can mitigate warming in the summer, especially during hot extremes (Hirsch et al., 2017; Nocco et al., 2019; Thiery et al., 2017, 2020). Furthermore, irrigation has also been found to affect precipitation and wind both locally, in intensely irrigated regions, and non-locally (Devanand et al., 2019; de Vrese et al., 2016; Saeed et al., 2009). As a result of expanding irrigation, irrigation-induced impacts on climate have also increased during recent decades (Puma & Cook, 2010; Thiery et al., 2020).

Irrigation is implemented differently in various land models. A simple implementation of irrigation consists of modifying the soil moisture directly without allowing for interception, infiltration and surface runoff, an approach which has been used in several models in the last decades (Kueppers et al., 2007; Ozdogan et al., 2010; Saeed et al., 2009; Telteu et al., 2021). Irrigation can also be modeled based on observed irrigation rates (Cook et al., 2015), or by calculation of water supply and demand (Guimberteau et al., 2012). There are also some models which calculate the irrigation demand according to the soil water deficit (Leng et al., 2017; Sacks et al., 2009; Thiery et al., 2017). In these implementations, irrigation is typically applied identically over all irrigated land regardless of whether or not there are difference in irrigation techniques used in different parts of the world or by different farmers. However, the amount, frequency, and method of water application directly influence the irrigation-induced impacts on water demand and climate (Leng et al., 2017). While several land and crop models now represent dynamic process-based irrigation methods including water conveyance and application processes (e.g., Jägermeyr et al., 2015; Valmassoi et al., 2020; Yin, Wang, et al., 2020), there is currently, to our knowledge, no Earth system model that represents such detail of different irrigation water withdrawal and application techniques. Thus, to detect the irrigation-induced impacts on the global hydrological cycle, energy budgets, and climate responses more realistically, improved irrigation modules in land surface models are needed which can (a) distinguish between different irrigation techniques, (b) be applied globally and (c) be coupled in Earth system models.

Community Land Model (CLM) was widely used in detecting irrigation-induced impacts(Sacks et al., 2009; Thiery et al., 2017; Zhu et al., 2020), but the representation of irrigation remains crude. In this study, we develop a new irrigation module including different irrigation techniques in the CLM, evaluate its performance relative to the original, generic irrigation module, and detect the influence on the water and energy cycles at the global scale. To this end, we first develop process-based representations of the two main irrigation techniques in CLM, including sprinkler and flood irrigation. The flood technique contains four different methods, three for rice crop types and one for other Crop Functional Types (CFTs). With a global distribution map of irrigation methods (Jägermeyr et al., 2015), we conduct five simulations, one with the original CLM irrigation scheme and four simulations with different combinations of the improved irrigation methods. In these simulations, different irrigation methods are used over cropland based on the distribution map, and water availability limitation is not represented. The simulated irrigation water withdrawal is then evaluated against observed amounts from US states, provinces of China and other countries. Based on the evaluation results of irrigation water withdrawal, the best combination of irrigation methods is selected as the new irrigation scheme. Next, the ability of this new scheme to reproduce evapotranspiration fluxes is evaluated at single-point scale for three cropland flux sites, in which sprinkler, flood and paddy irrigation techniques are used. At every single-point site, three simulations are conducted: one without irrigation, one with the original CLM irrigation scheme, and one with the new irrigation scheme. Subsequently, the effects of different irrigation methods on different components of evapotranspiration

and surface energy fluxes are detected. Finally, the irrigation-induced effects on global energy and water cycle with the new and the original irrigation module are detected by comparing them with simulations without irrigation and with each other.

2. Materials and Methods

2.1. CLM Model

The CLM is the default land component of the Community Earth System Model 2 (CESM2; Danabasoglu et al., 2020; Lawrence et al., 2019), which can be also used in land-only mode or coupled to other regional and global models (Zhu et al., 2020; Yin, Xu, et al., 2020). The currently released version CLM5.0 (hereby referred to as CLM) has several new features, including dynamic land unit weights, a mechanistic soil evaporation parameterization and the representation of land management (Lawrence et al., 2019). These new features have been successfully evaluated at global or regional scales (Fisher et al., 2019; Zhu et al., 2020) and show clear improvements relative to prior CLM versions, albeit with remaining weaknesses, like the representation of runoff in some catchments and the implementation of agricultural management (Cheng et al., 2021; Hirsch et al., 2018; Lawrence et al., 2019; Lombardozzi et al., 2020; Meier et al., 2019; Vanderkelen et al., 2022).

2.2. Original Irrigation Module

In the current version of CLM, there are two separated soil columns, rainfed and irrigated, for each CFT. A soil moisture dependent irrigation scheme is used, and its calculation is conducted individually over each irrigated column. The module is described in detail in Lawrence et al. (2018) and summarized hereafter. On every day at 6:00 a.m. local time, the model checks if the leaf area index (LAI) of crops is non-zero and if the available soil water over a given depth d_{root} (=0.6 m by default) is below a threshold. If both conditions are met, the irrigation scheme is activated. The threshold of soil water W_{thresh} (mm) is calculated as:

$$W_{thresh} = f_{thresh} \cdot (W_{target} - W_{wilt}) + W_{wilt} \tag{1}$$

where W_{target} (mm) is the target value of soil water, W_{wilt} (mm) is the soil water amount at wilting point, and f_{thresh} is a weight. W_{target}, W_{wilt}, f_{thresh} and d_{root} can all be adjusted by users. If $f_{thresh} = 1$, the model will irrigate once the available soil water is less than W_{target}, and if $f_{thresh} = 0$, the model will irrigate only when the available soil water is less than W_{wilt}. By default, $f_{thresh} = 1$. The W_{target} is calculated as the sum of target soil water of each soil layer:

$$W_{target} = \sum_{i=1}^{n_{irr}} \theta_{target,i} \cdot \Delta d_i \tag{2}$$

where n_{irr} is the index of the soil layer corresponding to d_{root}, Δd_i (mm) is the depth of the soil layer i and $\theta_{target,i}$ is the target volumetric soil moisture value. Similarly, W_{wilt} is calculated as the sum of soil water at wilting point of each soil layer:

$$W_{wilt} = \sum_{i=1}^{n_{irr}} \theta_{wilt} \cdot \Delta d_i \tag{3}$$

where θ_{wilt} is the volumetric soil moisture value at wilting point. θ_{target} and θ_{wilt} (here denoted as θ) are calculated by:

$$\theta = (\phi/\phi_{sat})^{(-1/B_i)} \cdot \theta_{sat} \tag{4}$$

where ϕ (mm) is the soil matrix potential parameter, which can be either ϕ_{target} and ϕ_{wilt} based on which volumetric soil moisture value we want to calculate (by default −3,400 and −150,000 mm, respectively). The target soil moisture calculated based on the default value of ϕ_{target} is meant to be field capacity. ϕ_{sat} (mm) and B_i are parameters related to the soil composition at soil layer i. The water applied for irrigation, W_{irr} (mm), is calculated as the deficit between W_{target} and the current soil water $W_{current}$ (mm):

$$W_{irr} = W_{target} - W_{current} \tag{5}$$

The water is evenly applied into the field during the irrigation time t_{irr} (s) (14,400 s by default), thus the irrigation speed a_{irr} (mm/s) is:

$$a_{irr} = W_{irr}/t_{irr} \tag{6}$$

The water is added into the rainfall under canopy (R_{under}, mm), so no interception is considered:

$$R_{under} = R_{under} + a_{irr} \cdot \Delta t \tag{7}$$

where Δt is the length of model time step. After being applied over the soil, the water used for irrigation experiences surface runoff, evaporation and infiltration. In CLM, the soil is represented as a multi-layer model, where water can transport vertically through different layers, and water in the root zone (0–0.6 m, first two layers) can be lost by canopy transpiration. Finally, the soil water arriving at the impermeable bedrock can generate sub-surface runoff. All the water used for irrigation is extracted from the main channel water storage in the routing model, or from the ocean in case the water demand cannot be met by this storage. The model also provides an option to limit the irrigation water amount by the availability of water in storage. By default, 90% of the water can be used for irrigation.

2.3. New Irrigation Techniques in CLM

Constrained by equipment, water availability and crop type, farmers irrigate with different techniques (Jägermeyr et al., 2015). In this study, we implement parameterizations for the two major irrigation techniques in CLM: sprinkler and flood. The flood irrigation methods are further separated for flood, paddy_1, paddy_2, and paddy_3 irrigation methods, and the last three methods are only used over rice paddies, as they are designed to store water on the surface. These parameterizations differ in their activation conditions, amount of water applied, method of application and surface water storage conditions. For all techniques, the activation conditions are checked only when crop LAI is non-zero.

The sprinkler technique is an irrigation method which is widely used in developed countries, especially in Europe and North America (Jägermeyr et al., 2015). Farmers use a system of pipes and sprayers to distribute water over the canopy of crops. In our implementation, the activation and amount of water used in sprinkler irrigation is the same as in the original scheme, but instead of being applied below the canopy, the irrigated water is added to the rainfall term above the canopy (R_{above}, mm):

$$R_{above} = R_{above} + a_{irr} \cdot \Delta t \tag{8}$$

In this way, part of the water is subject to canopy interception and evaporation before reaching the ground.

In most developing countries, flood irrigation remains the main technique, whereby farmers let water flow into the field through small trenches (Jägermeyr et al., 2015). Considering that the soil is normally saturated for a short period after flood irrigation, we change the amount of water applied for irrigation to the deficit between the soil water at saturation point and current soil water:

$$W_{irr} = W_{satu} - W_{current} \tag{9}$$

This representation of flood irrigation saturates the soil but does not allow for ponded water, so the water applied into fields lose quickly by surface runoff.

Rice is a CFT which is watered mainly by flood irrigation. However, rice periodically requires either storage of surface water in the field or drainage when the surface water depth is too high for the growth of crop (Bouman, 2007). To mimic this system, we therefore expand the flood irrigation technique to allow for pooling and drainage. We first develop a new water ponding module implementing storage and drainage for the three techniques of rice paddies (paddy_1, paddy_2, and paddy_3). In the current CLM irrigation module, there is a surface water variable, but it is related to natural topography and not suitable for human constructed rice paddies. In rice paddies, farmers usually modify local micro-topography to improve field water storage. We therefore modify the surface water scheme for rice paddies (both rainfed and irrigated) by keeping the surface water runoff to zero, thereby preventing surface water loss by runoff, so the water can be only lost by evaporation or infiltration. When

Table 1
Information on Irrigation Methods (All Parameters Are Described in Sections 2.2 and 2.3)

Method	Activation	Water amount	Place where water is applied	New water ponding module
Default	$W_{current} < W_{thresh}$	$W_{target} - W_{current}$	Under canopy	No
Sprinkler	$W_{current} < W_{thresh}$	$W_{target} - W_{current}$	Over canopy	No
Flood	$W_{current} < W_{thresh}$	$W_{satu} - W_{current}$	Under canopy	No
Paddy_1	$W_{current} < W_{thresh}$	$W_{satu} - W_{current}$	Under canopy	Yes
Paddy_2	$D_{sfc} < D_{th}$	$D_{\max} - D_{sfc}$	Under canopy	Yes
Paddy_3	$W_{current} < W_{satu}$	$W_{satu} - W_{current}$	Under canopy	Yes

the depth of surface water is more than the threshold (100 mm), which may limit the growth of rice, the drainage of surface water is activated and the extra water is removed in one time step:

$$Q_{sfc} = (D_{sfc} - D_{\max})/\Delta t \quad (10)$$

where Q_{sfc} is the surface water runoff (mm/s), D_{sfc} is the amount of surface water (mm), and $D_{\max}$ (=100 mm) is the maximum value of the surface water depth.

The parameterization of paddy_1 irrigation is the same as that of flood irrigation but uses the above mentioned new surface water ponding module. With this module, paddy_1 could store the water in fields better than flood irrigation when rainfall and irrigation occur.

For paddy_2 irrigation, watering is activated when surface water depth is less than a threshold (D_{th}: 10 mm), and the amount is the deficit between the target surface water depth (D_{tar}: 100 mm) and the current surface water depth D_{sfc}:

$$W_{irr} = D_{tar} - D_{sfc} \quad (11)$$

This way, paddy_2 irrigation effectively maintains a depth of 1–10 cm of water over the surface in rice paddies during the rice growing season.

For paddy_3 irrigation, the amount of water applied is the same as the paddy_1 technique, but irrigation is activated once soil water drops below the saturation point. Thus, with paddy_3 technique, irrigation is activated more frequently than with flood technique. Considering that the storage of surface water is normally realized by modifying the micro-topography, for all three paddy irrigation techniques we activate this ponding module throughout the entire simulation period, which means that in non-growing seasons, rainfall can also generate ponds in crop fields. This ponding module only exists over rice paddies. The settings of the different irrigation methods are summarized in Table 1.

Apart from sprinkler, flood and paddy irrigation, drip irrigation is another common irrigation technique. Drip irrigation is the most efficient method, allowing farmers to drip water slowly to the root zone of crops, ensuring the growth of crops while minimizing water use. Low conveyance and application losses make it an attractive technique where water is scarce (Van der Kooij et al., 2013). Considering that the drip technique is not widely used, we effectively use the default irrigation method in CLM5 as drip irrigation in this study (Section 2.2).

2.4. Experimental Design and Data

To identify the most skillful irrigation module, five global-scale land-only CLM5.0 simulations are designed, one with the old irrigation scheme (CTL) and others with different combinations of irrigation methods (Table 2). A new surface map data featuring a new variable, namely irrigation method, is generated based on the irrigation method distribution data from Jägermeyr et al. (2015). This distribution map provides the fraction of land equipped for different irrigation methods (drip, sprinkler and flood) of 16 CFTs at 0.5° × 0.5° resolution. For each of the 64 CFTs (32 rainfed and 32 irrigated) in the current version of CLM we select a corresponding CFT in the original data set (Table A1). To limit the computational cost of the irrigation module, we first resample the irrigation method distribution map to the target resolution, then simplify the surface map data by assigning each CFT in each pixel a single irrigation method (drip, sprinkler or flood) as the method with the largest area fraction of this CFT (some examples could be found in Figure 1). The flood technique over rice paddies can be replaced by paddy_1, paddy_2 or paddy_3 techniques in different simulations, and drip irrigation cropland is irrigated with the default irrigation scheme in CLM5. The simulations are forced by daily reconstructed meteorological data from the Global Soil Wetness Project Phase 3 (GSWP3, included variables can

Table 2
Global Community Land Model Simulation Settings for Irrigation

Simulation	Drip CFTs	Sprinkler CFTs	Flood CFTs[a]	Rice
CTL	Default	Default	Default	Default
IRR_0	Default	Sprinkler	Flood	Flood
IRR_1	Default	Sprinkler	Flood	paddy_1
IRR_2	Default	Sprinkler	Flood	Paddy_2
IRR	Default	Sprinkler	Flood	Paddy_3

[a]Excluding the rice Crop Functional Types (CFTs).

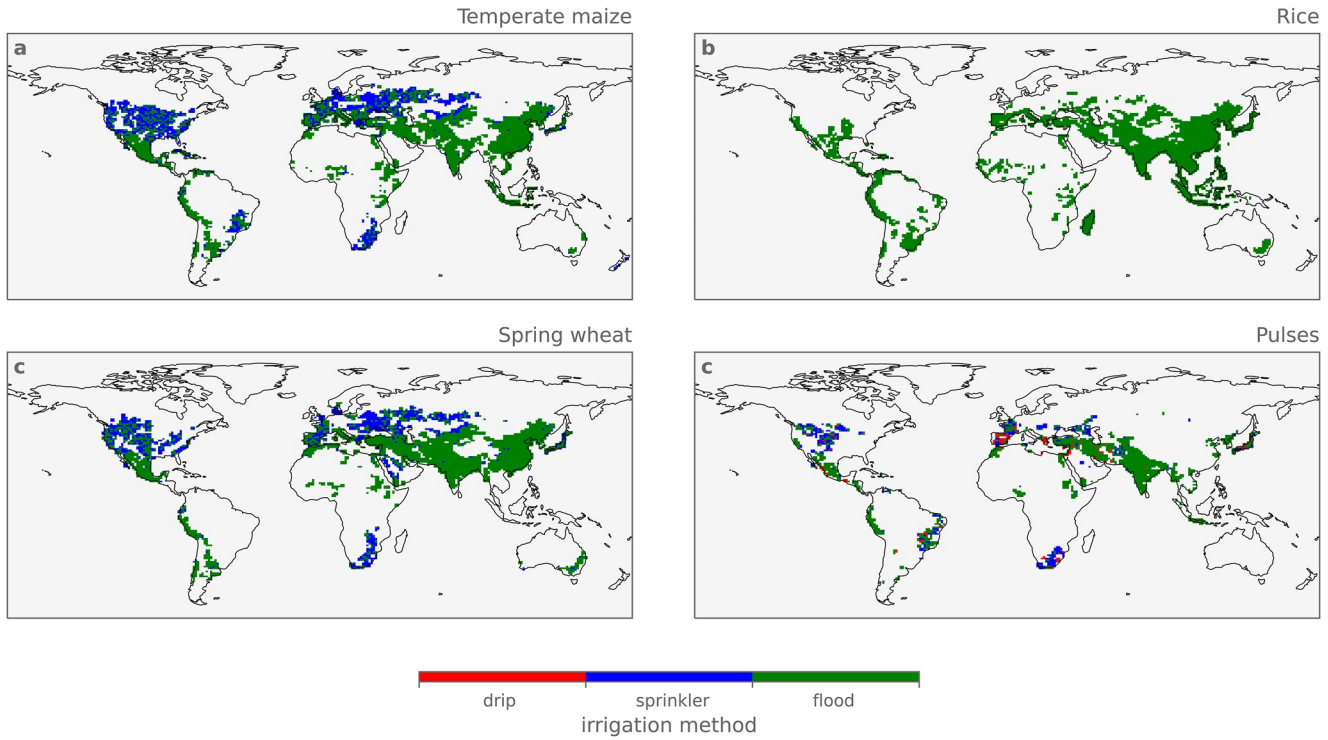

Figure 1. Irrigated crop and irrigation method distribution of temperate maize (a), rice (b), spring wheat (c) and pulses (d). The irrigated crop distribution is based on a data set of areas equipped for irrigation from Portmann et al. (2010). The irrigation method distribution is calculated based on the data set from Jägermeyr et al. (2015).

be found in Table A2). In all simulations, the water supply limitation is not activated, and if the irrigation water demand exceeds local runoff, CLM extracts the water from the ocean to close the water balance. In all simulations, all parameters in the irrigation module are assigned default values as described in Section 2.2. Land cover data used for simulations is the default data of CLM5 provided by National Center for Atmospheric Research (NCAR). The soil texture data is from the International Geosphere-Biosphere Program Data and Information System (IGBP-DIS).

The resolution of the global simulations is 0.9° × 1.25°, and the simulation period is 1981–2015, in which the first 5 years are used as a spin-up period. The irrigated area in CLM and irrigation technique distribution are both generated based on data around the year 2000, which is why the 30-year analysis period is centered around this year. The simulated irrigation water withdrawal at or near the year 2000 is compared to observations at the state scale in the USA, at the provincial scale in China and at the national scale in other countries following the availability of observational datasets (Table 3, Figure 2). For the global simulations, prognostic vegetation state and active biogeochemistry are activated, as simulations with satellite phenology assume a single CFT in the current version of CLM (Settings of the global simulations can be found in Table A3). Considering the different source of reference data in different regions, we calculate bias and root-mean-square error (RMSE) of irrigation water withdrawal separately in the USA states, China provinces and other countries, weighted by the observed irrigation water withdrawal. The reason for weighting the bias and RMSE is that the amount of observed irrigation withdrawal can be very different among different countries or regions, so averaging them evenly may not be appropriate.

Table 3
Source of Observed Irrigation Water Withdrawal

Country	Source	Year
The USA	USGS	2000
China	Zhou et al. (2020)	2000
Others	Aquastat	2002

$$bias = \sum_{i=1}^{n}(Q_{o,i} \cdot (Q_{s,i} - Q_{o,i}))/\sum_{i=1}^{n}(Q_{o,i}) \quad (12)$$

$$RMSE = \sum_{i=1}^{n}\left(Q_{o,i} \cdot \sqrt{(Q_{s,i} - Q_{o,i})^2}\right)/\sum_{i=1}^{n}(Q_{o,i}) \quad (13)$$

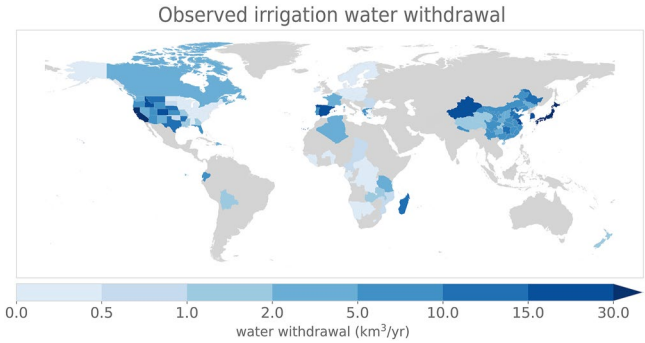

Figure 2. Observed irrigation water withdrawal per state (the USA), province (China) and country (others) during the early 21st century (2000 for the USA and China, 2002 for other countries).

where $Q_{o,i}$ (km^3) is observed irrigation water amount, $Q_{s,i}$ (km^3) is simulated irrigation water amount, and n is the number of states in the USA, provinces in China, or countries for other countries. Based on the results, the best performing combination of irrigation methods (IRR) is selected as the new irrigation module and used in the remainder of the analysis.

To detect the impact of the new irrigation scheme on the ability of CLM to simulate surface energy fluxes, we subsequently design several single-point simulations. Three sites from FLUXNET, Nebraska (NEB, USA), Castellaro (CAS, Italy) and Mase (MAS, Japan) are selected, as they represent three different irrigation techniques (sprinkler, flood and paddy). The site characteristics, including the crop type, irrigation method and simulation period, are listed in Table 4, while the location of the sites can be found in Figure 3b.

For every site, three simulations are designed, the first with the irrigation switched off (NOI), the second with the original irrigation scheme (CTL) and the third with the new irrigation scheme (IRR). Unlike in the global simulations, in the single-point simulations we use the LAI prescribed from satellite phenology (LAI data from Moderate Resolution Imaging Spectroradiometer [MODIS]), as there is only one CFT for each site and it allows us to exclude the impacts of different LAI between simulations and observations (settings of the single-point simulations can be found in Table A3). As CLM provides identical LAI data for all irrigated CFTs, this LAI data may be affected by other crops. To conduct these simulations, a single-pixel surface map data is prepared for each site, in which the land is set to be fully covered by the corresponding crop type. All meteorological forcing and data used for evaluation are generated based on in-situ observed data from FLUXNET (meteorological variables can be found in Table A2). To better understand the impacts of new irrigation techniques, we calculate and compare multi-year average monthly ET and its components (ground evaporation [GE], canopy evaporation [CE], and transpiration [TR]), and surface energy fluxes (latent heat flux [LHF], SHF, upwelling longwave radiation [LWup], upwelling shortwave radiation [SWup], ground heat flux [GHF], and Rnet) of three simulations. All simulations are repeated several times until the considered variables reach an equilibrium state. For all single-point simulations, the parameters in the irrigation module are also assigned default values as described in Section 2.2.

Finally, another global simulation without irrigation (NOI) is conducted for the same simulation period (1981–2015 with 1981–1985 as the spin-up period). The differences between those global simulations (NOI, CTL, and IRR) are used to analyze the irrigation-induced impacts on global water and energy cycle and the effects of IRR compared to CTL. To better understand the magnitude of irrigation-induced impacts, we calculate spatially-averaged effects at the global and regional scale. Selected regions are the IPCC climate reference regions with densely-irrigated croplands: Northern Central America (NCA), Mediterranean (MED), South Asia (SAS), East Asia (EAS) and Southeast Asia (SES; Figure 3a; Iturbide et al., 2020). Considering that these are land-only simulations, we only analyze irrigated areas within those regions (defined as all model grid cells with more than 10% irrigated land area). For all simulations, the water availability limitation mentioned in Section 2.2 is not activated, as the limitation is only based on surface water availability, whereas in reality, farmers extract not only natural surface water, but also groundwater and water stored or managed with agricultural infrastructures, such as reservoirs and canals. To quantify the effect of irrigation water extraction on runoff, we visualize this term as simulated runoff minus local irrigation water withdrawal.

Table 4
Information of Flux Sites

Sites	Latitude (°)	Longitude (°)	Crop type	Irrigation method	Period	Reference
Nebraska (NEB)	41.1649	−96.4701	Maize	Sprinkler	01/2001–12/2013	Suyker (2001–2013)
Castellaro (CAS)	45.0700	8.7175	Maize	Flood	01/2009–12/2010	Manca and Goded (2009–2010)
Mase (MAS)	36.0539	140.0269	Rice	Paddy_3	04/2012–12/2012	Iwata (2012)

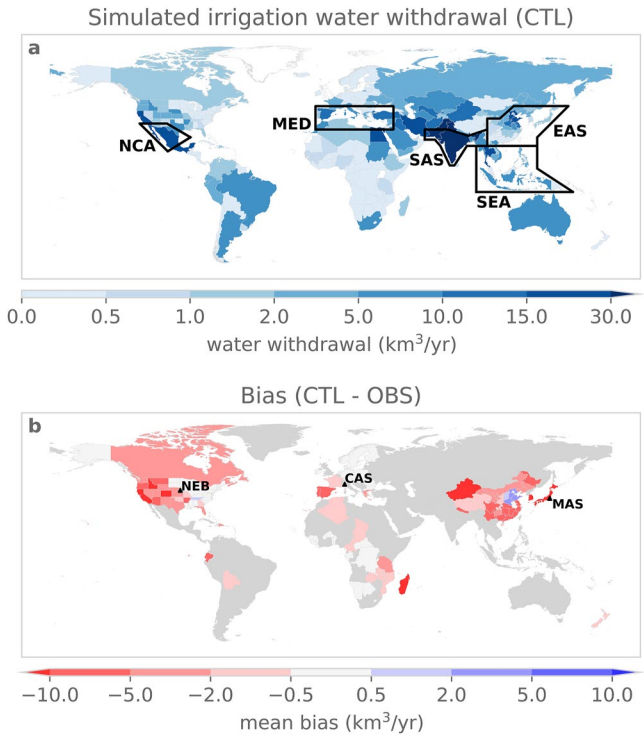

Figure 3. Simulated irrigation withdrawal with the original irrigation module (CTL) and the regions used in regional analysis (NCA: northern central America; MED: Mediterranean; SAS: South Asia; EAS: East Asia; SEA: Southeast Asia) (a); the bias compared to observations and the location of the sites used in single-point simulations (NEB: Nebraska; CAS: Castellaro; MAS: Mase) (b). Comparisons are made using withdrawals computed around the year 2000: the USA (2000), China (2000) and other countries (2002). The regions in gray are missing observed irrigation quantities.

3. Results

3.1. Evaluation of Irrigation Water Withdrawal

In almost all regions worldwide, CTL underestimates observed irrigation water withdrawal (Figure 3). In the original irrigation scheme of CLM, irrigation is only activated when crops experience water stress, and the quantity of water applied is limited by the deficit between target soil water and actual soil water, which is the main reason for the general underestimation. This impact is more pronounced in the regions densely covered by rice paddies, including Japan, Madagascar, and South Korea, where the underestimation exceeds 10 km^3/yr nation-wide, as rice paddies have large irrigation water requirements. In total, the weighted average underestimation amounts to 10.58 km^3/yr per state in the USA, 5.15 km^3/yr per province in China and 64.74 km^3/yr per country for other countries (Table 5).

Exceptions to this general pattern occur mainly in northern central China, where CLM slightly overestimates the irrigation water withdrawal (Figure 3). One possible reason for this is that in this region the agricultural land is densely distributed, and the irrigation demand exceeds the available water amount, while in our simulations the limitation of water availability is not enabled.

All four irrigation method simulations increase the irrigation water withdrawal over most regions, but to varying degrees (Figure 4). The biases shift from −10.58 to −4.21, −4.21, −0.03, and +8.49 km^3/yr per USA state in IRR_0, IRR_1, IRR, and IRR_2, respectively, from −5.15 to 3.26, 3.25, 22.34, and 70.94 km^3/yr per Chinese province, and from −64.74 to −33.08, −33.08, −7.67, and 104.14 per country for other countries. While there are only negligible differences between IRR_0 and IRR_1, simulated irrigation water withdrawals are slightly higher in IRR_0.

Underestimations still occur for IRR_0 and IRR_1 over most regions, while overestimations in central China are enlarged (Figure 4). Additionally, in places like Texas, France and Northern China, there is a transition from underestimating irrigation amounts to overestimating them. In total, IRR_0 and IRR_1 decrease the weighted underestimations by ∼50% in the USA and other countries, and reverse the underestimation in China to a slight overestimation.

The IRR_2 and IRR simulations both substantially increase the irrigation water withdrawal over most regions, resulting in substantial overestimations in some regions, especially in Madagascar, California, Equator and some Chinese provinces (Figure 4). This is due to the high demand of water in IRR_2 (required for maintaining a target depth of surface water) and the high frequency of irrigation in IRR (as irrigation is activated as soon as soil moisture falls below the saturation point) over rice paddies. For IRR_2, we find substantial overestimation of

Table 5
The Criteria (Weighted Bias and Root-Mean-Square Error, RMSE) of Simulated Irrigation Water Withdrawal

	CTL		IRR_0		IRR_1		IRR_2		IRR	
Country	Bias	RMSE	Bias	RMSE	Bias	RMSE	Bias	RMSE	Bias	RMSE
USA	−10.58	13.42	−4.21	**6.56**	−4.21	**6.56**	8.49	25.16	**−0.03**	7.94
China	−5.15	**7.38**	3.26	10.84	**3.25**	10.84	70.94	111.57	22.34	29.84
Others	−64.74	78.79	−33.08	39.22	−33.08	39.22	104.14	140.84	**−7.67**	**14.4**

Note. For the USA (2000) and China (2000), the criteria were calculated based on the annual data at state or province scale, and for other countries (2002), the calculation is based on annual data at the national scale (unit: $km^3\ yr^{-1}$). The bold values indicate the simulation with the best performance.

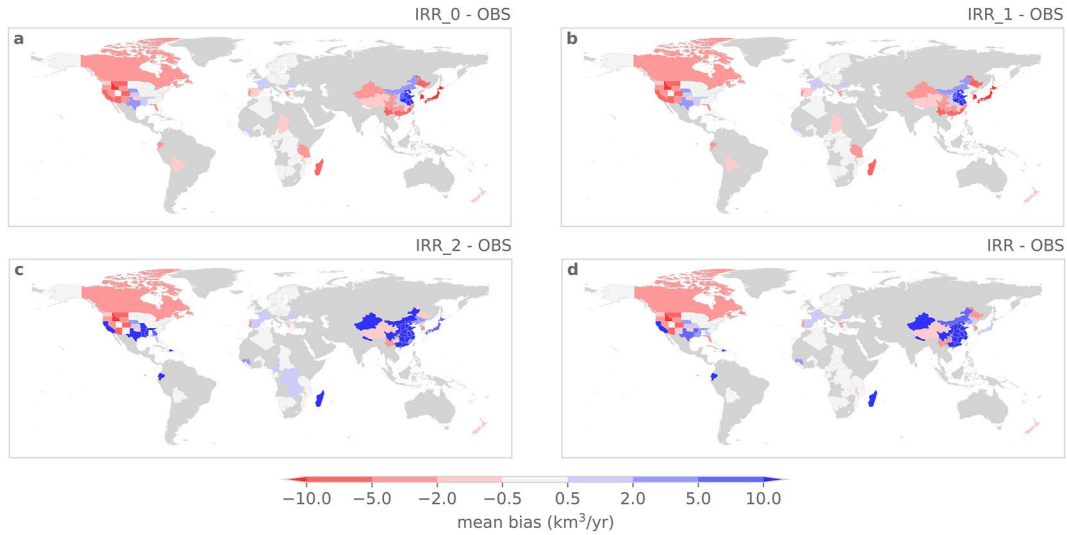

Figure 4. Bias of irrigation water withdrawal of the four simulations: IRR_0 (a), IRR_1 (b), IRR_2 (c) and IRR (d). The biases are the value around year 2000, the USA (2000), China (2000) and other countries (2002). Positive values indicate overestimation of irrigation water withdrawal.

irrigation water withdrawals worldwide, while for IRR, this overestimation is less pronounced. At the same time, although underestimations still exist in some regions in IRR, they are notably reduced, and in several regions, this bias is limited in a small range. Numerically, IRR_2 greatly overestimates the irrigation water withdrawal in the USA, China and other countries, while IRR almost eliminates errors in the USA, substantially decreases the bias in other countries, but turns a slight underestimation to a large overestimation in China.

Globally, the worldwide irrigation water withdrawal amounts to ~910 km^3/yr for CTL, ~1,900 km^3/yr for IRR_0 and IRR_1, ~3,600 km^3/yr for IRR and ~7,700 km^3/yr for IRR_2. According to previous studies, the global irrigation water use around the year 2000 ranges in 2800–3,000 km^3/yr (Hanasaki et al., 2008; Wisser et al., 2010). IRR_2 is not considered in the remainder of the analysis due to its high bias. IRR_0, IRR_1 and IRR all decrease the bias over most regions and approach the global irrigation water withdrawal range obtained from previous research, but IRR_0 does not represent surface water storage in rice paddies, and IRR_1 cannot keep the soil water at a near-saturated level in rice paddies during the growing season. Moreover, considering that the water availability is ignored in these simulations, we think a reasonable overestimation of the global irrigation water withdrawal (as in IRR) is to be preferred over an underestimation (as in IRR_0 and IRR_1). For these reasons, we select IRR as the new irrigation scheme.

3.2. Evaluation and Analysis of Land Fluxes in Single-Point Experiments

While all simulations generally capture the seasonal pattern at three sites (Nebraska, NEB; Castellaro, CAS; Mase, MAS; Figure 5), there are some mismatches in magnitude. In Nebraska, simulations slightly overestimate ET in May and underestimate ET in other months, while at the other two sites, the model greatly underestimates ET across the whole year, especially during June-August. One possible reason for these unmatched results is the uncertainty in prescribed LAI, as in CLM, the LAI used for prescribed phenology simulation is generated from satellite cropland LAI, which includes the LAI of other CFTs (as mentioned in Section 2.4). At the same time, the meteorological data used to force the model is based on observations from the same flux site, which may already include atmospheric feedbacks of irrigation activities, while our land-only simulations cannot take the interactions between land and atmosphere into account. This could potentially explain the underestimation of ET in Castellaro and Mase, as the vapor pressure deficit may have already been decreased by irrigation. Using satellite LAI data can also explain the unrealistic irrigation water use seasonality in Mase, as non-zero crop LAI is a condition for activating irrigation.

The IRR simulation increases ET, while the effects are relatively limited, with the maximum monthly differences amounting to 0.47 mm/day in Nebraska, 0.08 mm/day in Castellaro and 1.10 mm/day in Mase (Figure 5). The

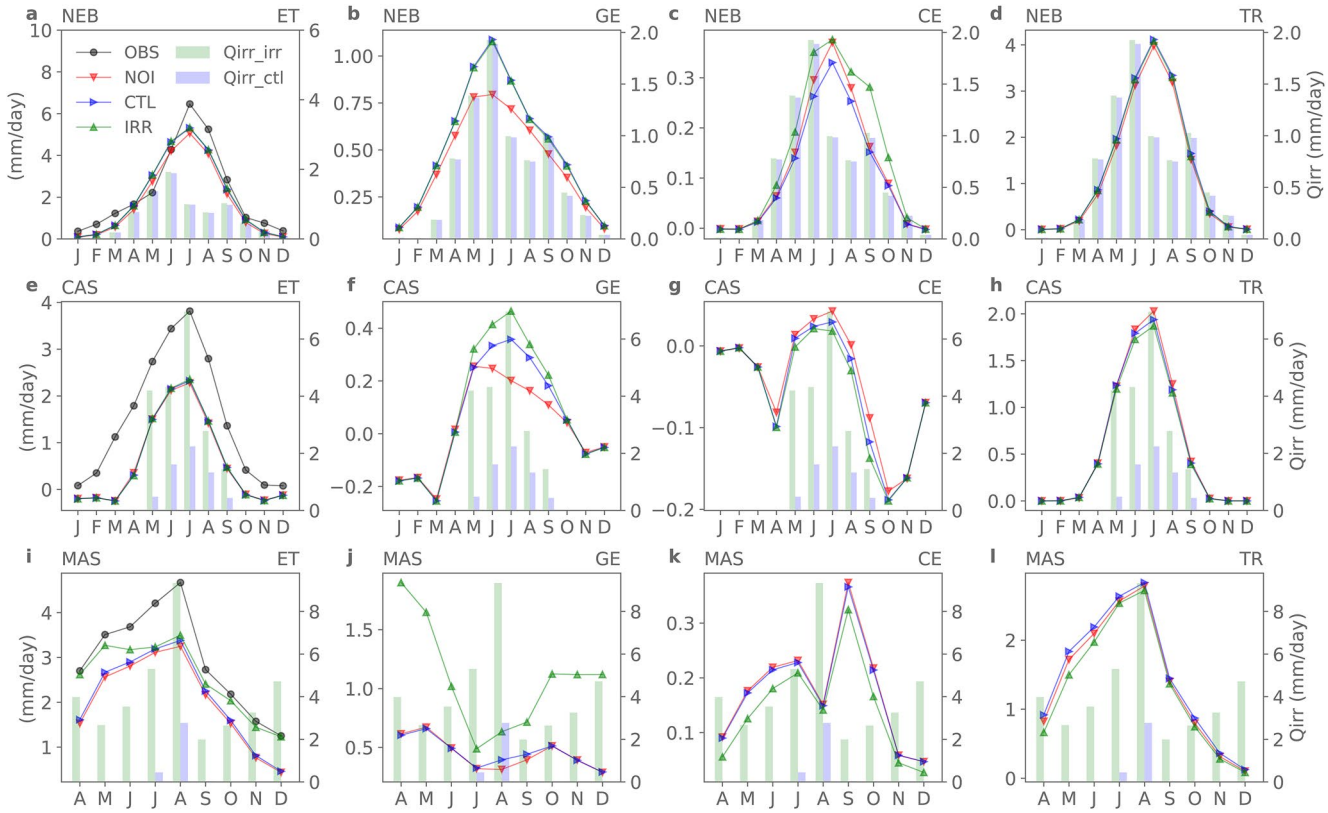

Figure 5. Multi-year average monthly observed evapotranspiration (ET) (black line), simulated evapotranspiration, ground evaporation (GE), canopy evaporation (CE) and transpiration (TR) of NOI (red lines), CTL (blue lines) and IRR (green lines), and simulated irrigation water amount (Qirr) of CTL (blue bars) and IRR (green bars) in Nebraska (NEB), Castellaro (CAS) and Mase (MAS). The simulation periods can be found in Table 4.

seasonal patterns of these irrigation-induced impacts are in line with the simulated irrigation quantity (green bars) in Nebraska and Castellaro. Conversely, in Mase, the impacts are more pronounced in April and December, and the least substantial in July and August, when the most water is applied for irrigation. Interestingly, the increased ET in April, May, September to December is more similar to observations, while in other months substantial underestimation remains.

The impacts of irrigation with the new irrigation module (IRR-NOI) on ET components (GE, CE, and TR) vary among sites (Figure 5). In Nebraska, three variables have similar seasonal patterns, and are all increased by irrigation. Impacts on GE are in line with the irrigation amount, as GE is directly related to soil water, so the increase in GE is the main contributor of the increased ET in peak month (0.28 mm/day in June). Impacts on CE follow the same pattern, since more irrigation water means more interception when sprinkler irrigation technique is used, but the effect is most pronounced in September (0.12 mm/day). One possible reason is that in July and August, GE and TR are greatly increased, resulting in a higher air humidity at canopy height, which constrains CE, while in September, the increased GE and TR are less substantial than in July and August, but irrigation water application is still at a high level. The increase in TR remains steady between April and August (0.11–0.13 mm/day), due to the high LAI and alleviated water stress by irrigation (Figure A1). In Castellaro, irrigation is only activated from May to September, thus irrigation-induced impacts on all variables are more pronounced in this period. Irrigation increases GE, but slightly decreases CE and TR, which is why irrigation-induced impacts on ET in Castellaro are very limited. Irrigation water increases soil moisture, then facilitates GE, and shifts the peak from May to July, the month when the most water is applied. However, increased air moisture and decreased temperature at canopy height caused by GE may in turn reduce CE and TR. Impacts on GE and TR are highly related to the amount of irrigation water (0.26 and −0.16 mm/day in July, respectively), but similar to Nebraska, impacts on CE are more pronounced in September (0.05 mm/day). In Mase, irrigation is activated every month from April to December, and causes a great increase in GE and a small decrease in CE and TR. In paddy_3 irrigation, rice paddies are designed to prevent water loss through surface runoff, which causes GE to increase substantially. Interestingly,

the seasonal pattern of GE is altered by irrigation, with high values from April to June (0.52–1.28 mm/day) and October to December (0.61–0.83 mm/day), and with low values from July to September (less than 0.33 mm/day). One possible reason is that high LAI during June-September (Figure A1) decreases the shortwave radiation absorbed by the ground, so the increase in GE is limited compared to in other months. Similar to other sites, increased GE then restrains CE and TR with a limited magnitude, and the peaks are in May and in October for CE (−0.05 mm/day) and in May for TR (−0.22 mm/day).

At all three sites, the impact of the irrigation on ET in IRR is more pronounced than in CTL (IRR-CTL), and the difference is small in Nebraska and Castellaro, but large in Mase (Figure 5). In Nebraska, the new scheme slightly increases the water used for irrigation, as water application over canopy in sprinkler method has interception loss before reaching the ground, causing lower soil moisture and slightly higher irrigation demand. This limited difference has small effects (on ET), less than 0.06 mm/day in peak months. The difference in GE is negligible, but CE is substantially increased by the new scheme due to the increased interception, while TR has little change, as root zone (top 0.6 m) soil moisture shows little difference between two schemes (Figure A1). In Castellaro, irrigation is activated from May to September in both CTL and IRR, but the new scheme substantially increases the water amount applied. However, the impact of the increased irrigation water on ET is small (less than 0.03 mm/day). Compared to the old scheme, the increased water applied for irrigation by the flood technique provides more root zone soil water shortly after the irrigation (Figure A1), causing a higher GE. In contrast, CE is decreased by a small amount, as water is applied under the canopy in the flood method (i.e., there is no change in interception). TR is decreased, possibly due to the same reason as in Nebraska. In Mase, not only irrigation water is increased in IRR, but also the irrigation period is prolonged, as the condition for activating irrigation is easier to meet in the new scheme. The new irrigation scheme greatly increases the irrigation-induced impacts on ET compared to the old scheme (up to 1.01 mm/day). This is due to the new ponding module of the paddy_3 irrigation method and the associated increased water applied. Rice paddies are able to hold surface water, and the root zone soil moisture is kept at a higher level (Figure A1) every time step, which substantially increases GE, which is the main contributor of the increase in ET. However, IRR decreases CE and TR compared to CTL, which may also be due to the increased air moisture and decreased temperature at canopy height caused by increased GE.

At all three sites, CLM generally reproduces LWup, but the performance of simulating SHF and SWup is poor (Figure 6). At all sites, observed SHF shows sharp decreases in months with intense irrigation (June-August in Nebraska and Castellaro, July-August in Mase), but the model does not reproduce them. Generally, the impacts of irrigation on SHF (IRR-NOI) and the difference between the original and the new irrigation module (IRR-CTL) are opposite to its impacts on LHF, but with a smaller magnitude, and Mase remains the most affected site, especially during April-May and October-November. Simulations in Nebraska and Mase both overestimate LWup slightly (there are no LWup observations in Castellaro), and irrigation decreases LWup (IRR-NOI). This decrease is more pronounced in Mase during April-May and October-November, which greatly reduced the bias. As for SWup, CLM overestimates the observed values at all three sites, possibly due to the model's poor ability to reproduce the surface albedo or because of uncertainties in the prescribed LAI data. The impacts of irrigation on SWup are negligible because phenologies are prescribed in the single-point simulations, irrigation therefore has little impact on surface albedo. To better understand the surface energy balance, we also plot downwelling shortwave radiation (SWdown) and downwelling longwave radiation (LWdown) (as forcings obtained from reanalysis), simulated GHF and Rnet (Figure A2). The impacts of irrigation on GHF and Rnet are small in both Nebraska and Castellaro, but there are pronounced impacts in Mase. With the original irrigation module (CTL), the impact of irrigation on Rnet is generally small, while with the new module (IRR), the influence is more pronounced, especially during April–May and November–December when Rnet increases, mainly due to the decreased LWup. For GHF, the differences between the three simulations are time-varying. Compared to NOI, CTL simulates a lower GHF throughout the simulation period, as it has a higher LHF. However, IRR reports a higher GHF during June-August, which can be attributed to the increased Rnet, while after September, GHF falls less than NOI and CTL due to the increase in LHF.

Overall, the new irrigation methods have limited impacts on ET, except paddy_3 irrigation in non-peak season, when the ET increased substantially and now much better matches with the observations. When splitting the impacts on ET to those on GE, CE and TR, we find that the three new methods have seasonally varying effects on the ET components. Irrigation has opposite, but smaller impacts on SHF compared to LHF (ET). The impacts of irrigation both with the original and the new irrigation module are small on radiation fluxes except in Mase.

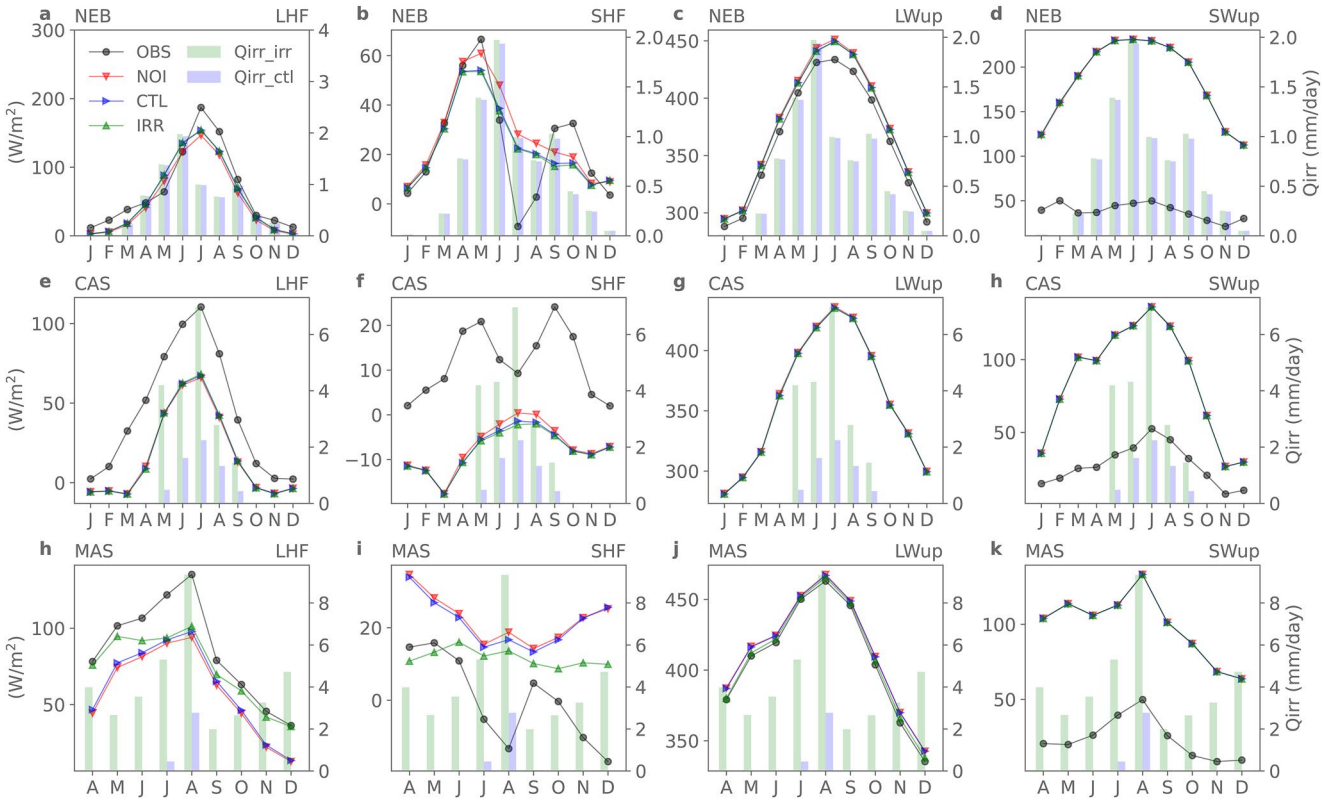

Figure 6. Multi-year average monthly observed (black line) and simulated latent heat flux (LHF), sensible heat flux (SHF), upwelling longwave radiation (LWup) and upwelling shortwave radiation (SWup) of NOI (red lines), CTL (blue lines) and IRR (green lines), and simulated irrigation water amount of CTL (blue bars) and IRR (green bars) in Nebraska (NEB), Castellaro (CAS) and Mase (MAS). The simulation periods can be found in Table 4.

3.3. Irrigation-Induced Impacts on Water Cycle and Energy Budget

In a global-scale, land-only simulation using the new irrigation module (IRR), evaporation (E: GE + CE), TR and total column soil water (TSW) generally increase over irrigated land, whereas runoff (R: calculated as runoff minus irrigation water withdrawal) decreases (IRR-NOI: Figure 7). Compared to the impacts of the original module (CTL), there is little change in the spatial pattern of these effects: the most pronounced effects occur over densely-irrigated lands, such as India, central China and western USA (CTL-NOI: Figure A3). However, the magnitude of the effects between IRR and CTL notably differs, whereby IRR has larger impacts for most of the variables (IRR-CTL: Figure A5). Compared to the original module, more *R* is extracted and applied into agricultural fields with the new module, which increases TSW and in turn stimulates more E. The effect on TR is more complicated, as the new irrigation module decreases TR over most of the irrigated land, and even reverses the sign of irrigation-induced impacts on TR in some pixels over central China. Possible reasons for the suppressed TR include the increased near-surface moisture and decreased temperature via higher E or the changes in crop phenology caused by irrigation.

Regarding energy fluxes, Irrigation enhances LHF, and reduces SHF, SWup, and LWup, and these impacts have a similar spatial pattern as the impacts on hydrological variables (Figure 8). In our study we did not couple CLM with an atmospheric model. Therefore, the decrease in LWup may be attributed to the cooling effect of irrigation on land surface temperature, as LWup has a positive correlation with land surface temperature. In global simulations, the impacts of irrigation on SWup are minor, and the effects can be attributed to the changes of the phenology of crops, which may together decrease the surface albedo. IRR also demonstrates stronger impacts compared to CTL, but overall, the magnitude of the difference between the impacts of two irrigation schemes (IRR-CTL) is less pronounced than the effect of switching on the original irrigation scheme (CTL-NOI; Figure A4 and A6).

To quantify these irrigation-induced impacts, we calculate the spatially averaged difference in variables between NOI, CTL, and IRR over global and regional irrigated land (Figure 9). Compared to NOI, CTL substantially

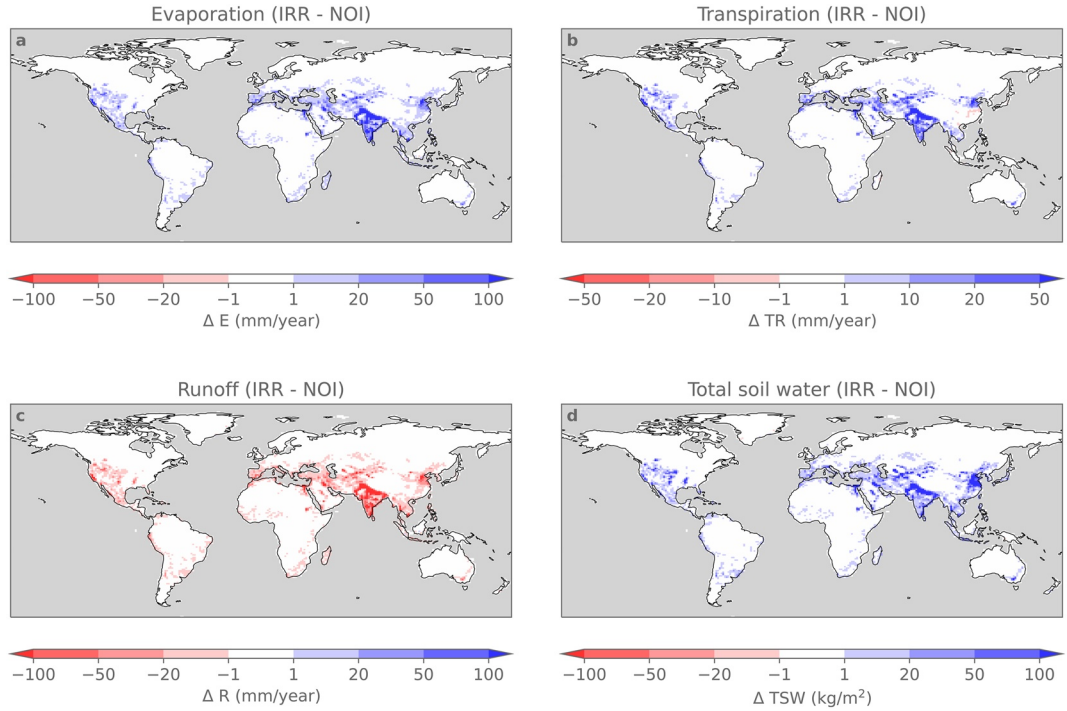

Figure 7. Impacts of irrigation (IRR-NOI) on the water cycle, including evaporation (a), transpiration (b), runoff (c) and total column soil water (d) for the period 1986–2015. Runoff plotted here is calculated as runoff minus irrigation water withdrawal.

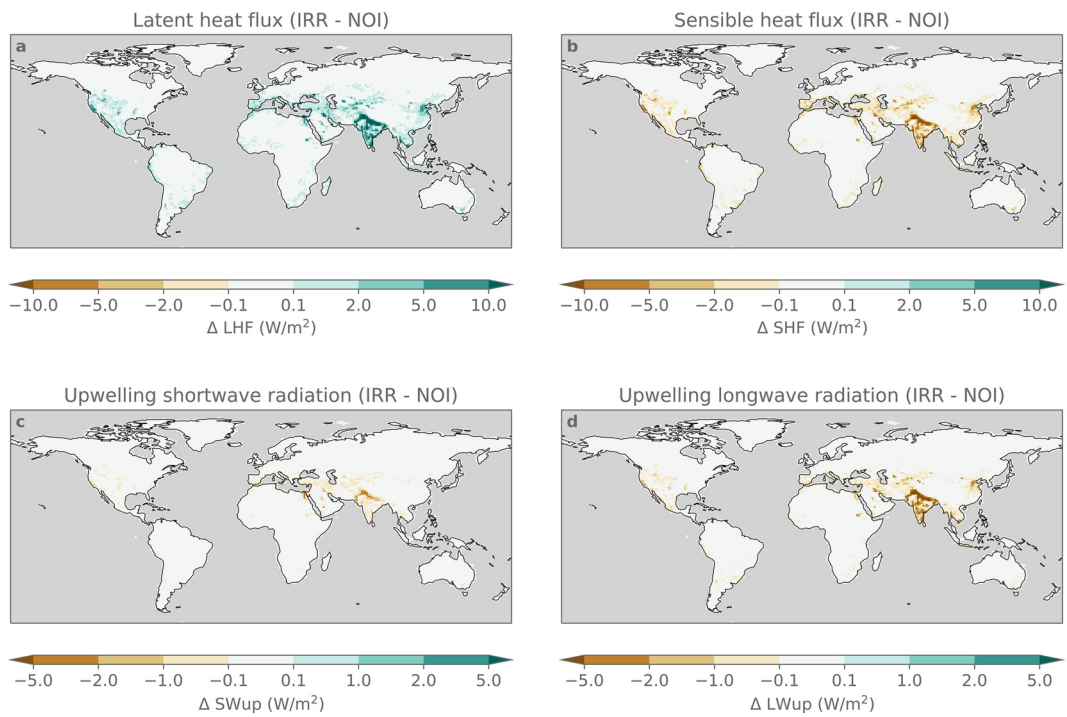

Figure 8. Impacts of irrigation (IRR-NOI) on the energy cycle, including latent heat flux (a), sensible heat flux (b), upwelling shortwave radiation (c) and upwelling longwave radiation (d) for the period 1986–2015.

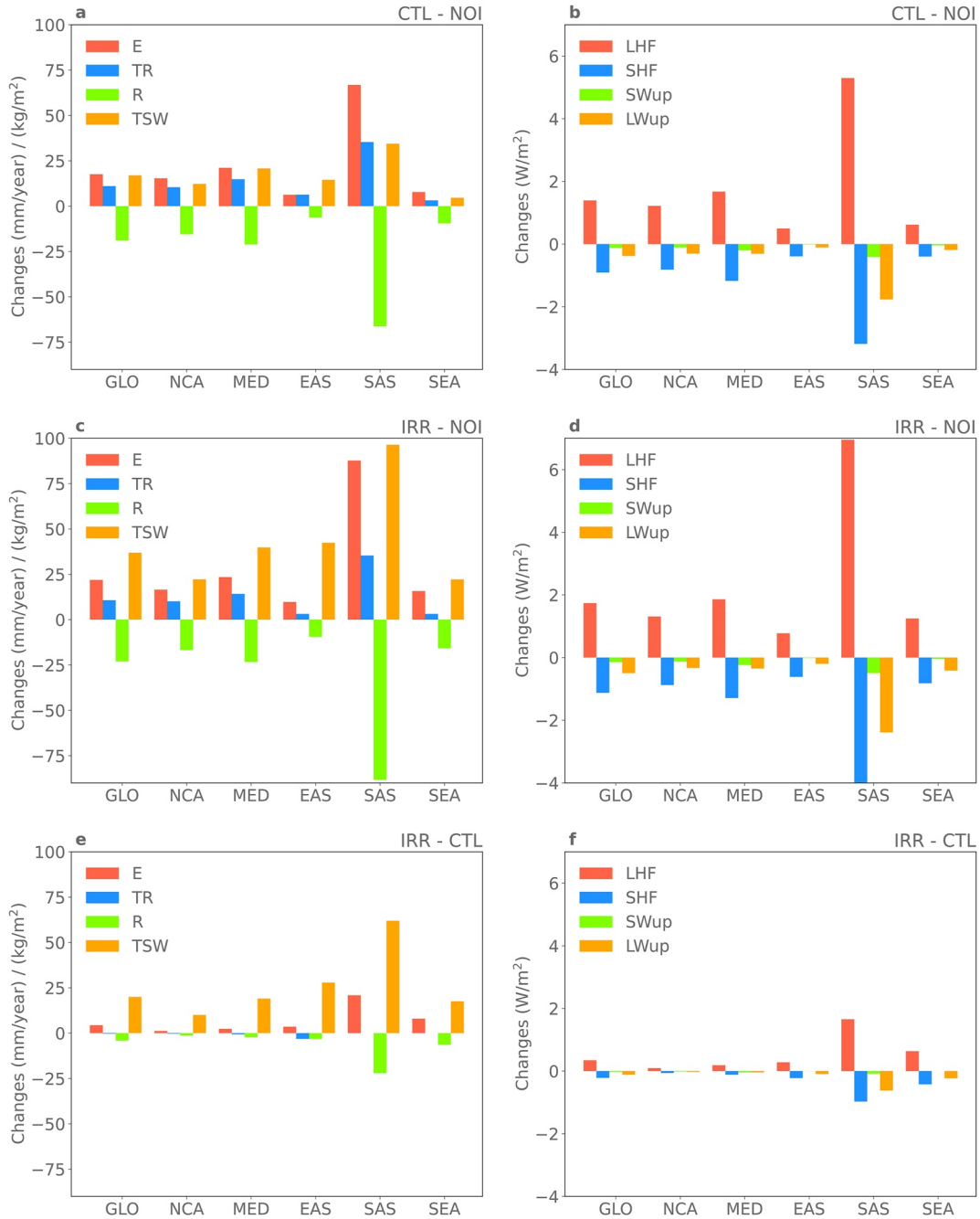

Figure 9. Spatial mean changes in evaporation (E, mm/year), transpiration (TR, mm/year), runoff (R, mm/year) and total column soil water (TSW, kg/m^2) (a, c, e), latent heat flux (LHF, W/m^2), sensible heat flux (SHF, W/m^2), upwelling shortwave radiation (SWup, W/m^2) and upwelling longwave radiation (LWup, W/m^2) (b, d, f) between the simulations CTL and NOI (a) and (b), IRR and NOI (c) and (d), IRR and CTL (e) and (f) over global (GLO) and regional irrigated land (pixels with more than 10% irrigated land): Northern Central America (NCA), Mediterranean (MED), South Asia (SAS), East Asia (EAS) and Southeast Asia (SES) for the period 1986–2015.

increases E (~18 mm/yr), TR (~11 mm/yr) and TSW (~17 kg/m^2), and reduces R (~-19.0 mm/yr). As the most densely irrigated region, SAS is the region where the impacts are the most pronounced with a decrease at ~66 mm in R per year, and an increase of ~67 mm in E, ~35 mm in TR and ~34 kg/m^2 in TSW per year. Other regions where the effects occur, albeit less substantial, are NCA, MED, and EAS and SEA. Similar results are also found for energy budget variables. CTL increases LHF by 1.4 W/m^2 relative to NOI, and decreases SHF,

SWup and LWup by ~0.90, ~−0.12, and ~−0.38 W/m^2 over global irrigated land, respectively. In SAS, these impacts are intensified to 5.3, −3.2, −0.4, and −1.8 W/m^2, respectively.

Compared to CTL, IRR shows stronger impacts on the water cycle (Figure 9). Over global irrigated land, IRR increases E by ~4.3 mm/yr and TSW by ~20 kg/m^2, while TR decreases by ~−0.3 mm/yr and R by ~4.1 mm/yr compared to CTL. The relative change between IRR and CTL is very pronounced for TSW, as the new irrigation scheme greatly improves the quantity of water applied into the field, and the new ponding module for rice paddies prevents more water from being lost as runoff. Impacts on E and TR are consistent with the results of the single-point experiments (Section 3.2): E increased and TR slightly decreased. Despite the rise in water extraction for irrigation, the impacts of the new irrigation scheme on R are also small, as a considerable part of the water applied in the field, except rice paddies, is lost as return flow. Due to its densely distributed rice paddies, SAS remains the region where the new irrigation scheme most strongly affects all variables, and interestingly, the difference of E and R between CTL and IRR are larger in SEA than in NCA, MED, and EAS, although the difference between NOI and CTL are less pronounced in this region. The reason may be that in CTL, irrigation demand is very small due to local meteorological conditions, whereas in IRR, more water is applied for irrigation, contributing to enhanced influences. In addition, the main crop type in this region is rice, and paddy_3 irrigation has more pronounced impacts than other methods.

Similar intensifying effects of IRR are also found when considering the surface energy balance (Figure 9). The irrigation-induced impacts on four surface energy fluxes are all increased in the new irrigation scheme, and amount to ~0.34, ~−0.22, ~−0.03 W/m^2 and ~-0.12 W/m^2 for LHF, SHF, SWup, and LWup, respectively, over global irrigated land (Figure 9). Among them, turbulent heat fluxes experience stronger changes than upwelling radiation fluxes, and the reason may be that compared to the turbulent heat fluxes, the radiative fluxes are less directly affected by the irrigation water amount but more constrained by other factors (e.g., land cover). Additionally, the changes in radiative fluxes might be larger in a coupled simulation that allows for dynamic atmospheric responses. As with the effects on water cycle, SAS is the region where the impacts are most pronounced, and the influence on the energy budget is also stronger with the new irrigation scheme in SEA than in NCA, MED, and EAS.

The irrigation-induced impacts on hydrology and energy vary across different periods of the year (Figures 10 and 11 and Figures A7, and A8). Over global irrigated land, both IRR and CTL increase E, TR, and LHF, decrease SHF, LWup, and SWup in the peak growing season (May–September), but in other months, these impacts are less noticeable. This is because most of irrigation water is applied in these periods. Unlike these variables, TSW is increased over the whole year, and the impacts in July are slightly more pronounced than in other months. R is decreased in April–July, then increased in August–January. The reason is that during growing seasons, water is extracted for irrigation; then in other months, the increased soil moisture decreases the infiltration rate when rainfall occurs. The irrigation-induced impacts on all variables except R do not change their seasonal pattern in most of the regions. The only exception is SAS, where the great increase in E, TR and LHF during the growing season even alters the seasonal patterns, shifting the peak of E and LHF from October to June, and the peak of TR from May to June.

Overall, most of the irrigation-induced effects in the water and energy cycle are enhanced when switching from the original to the new irrigation scheme, while the spatial patterns of these impacts generally do not change. The magnitude by which these variables change differs between regions, but in each case, SAS remains the region that is the most influenced by the new irrigation scheme. Compared to regions like NCA, MED and EAS, SEA appears more sensitive to the switch to the new irrigation scheme due to densely distributed rice paddies in this region. Irrigation could alter the seasonal pattern of R, while for other variables, the impacts on seasonal cycle are small, except for evapotranspiration in SAS.

4. Discussion

The original irrigation module of CLM was found unable to reproduce irrigation water withdrawals accurately in SEA and EAS (Thiery et al., 2017). Prior studies have bridged this gap by calibrating the target soil water, and found that in East USA, South China and some countries in SEA, the optimal target soil water is near to the saturated value, which is the case of the flood technique in our development (Leng et al., 2015). Due to the underestimation of irrigation water withdrawals in the original scheme in some densely irrigated lands, like SEA, the simulated irrigation-induced impacts on climate were not pronounced in those regions when using earlier

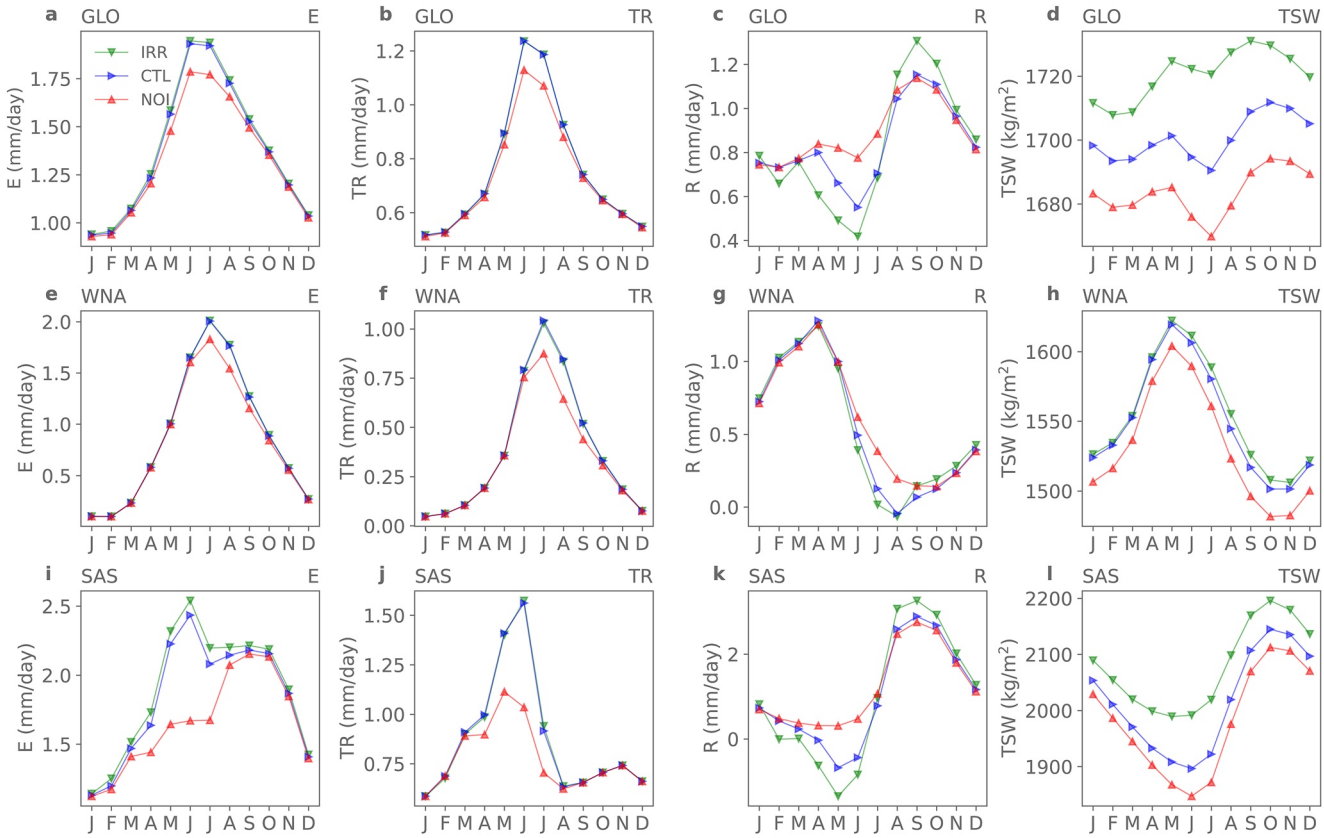

Figure 10. Multi-year average monthly simulated evaporation, transpiration, runoff and total water storage over global (GLO; a–d), Western North America (WNA: e–h) and South Asia (SAS: i–l) irrigated land. The analysis period is 1986–2015. Runoff plotted here is calculated as runoff minus irrigation water withdrawal.

versions of CLM (e.g., Thiery et al., 2017). With the new irrigation module, the irrigation-induced impacts in this region are larger. Results also report an unrealistic overestimation over North central China. Previous research shows that in this area, due to irrigation water use, the groundwater table has been decreasing in the past two decades (Wang et al., 2019). This indicates that farmers face water scarcity in this region. A regional study with the ORCHIDEE land surface model found a similar overestimation in the same region and showed that implementing a water availability limitation could alleviate the bias (Yin, Wang, et al., 2020). This contrasts with other regions where irrigated areas are less dense, or where water storage techniques like reservoirs and canals can more readily ensure that the irrigation demand can be met.

Despite the various effects of different irrigation methods, there is a consistency of decrease in SHF and increase in LHF. Several previous studies have also highlighted the decrease in the ratio of SHF and LHF (Bowen Ratio) (Chen & Jeong, 2018; Cook et al., 2015; Thiery et al., 2017), as the added water by irrigation can absorb more energy while evaporating. Moreover, there is also consistency of irrigation-induced impacts on longwave radiation. Cook et al. (2011) and Cook et al. (2015) report increase in net longwave radiation with coupled simulations, which has also been found in this study (fixed LWdown and decreased LWup).

While the newly developed irrigation module improves irrigation water withdrawal, some limitations still exist in this study. First, simulating irrigation using the original or new scheme does not dramatically improve the performance in simulating land fluxes at single-point sites. The impact of irrigation on most variables has a positive correlation with the amount of water used for irrigation, but whether it can improve the model performance varies across the sites. To improve our understanding of the new irrigation scheme's impacts on site-specific land fluxes and hydrological variables, more sites in different regions, with different crop types and irrigation methods, should be used for further study. However, a major issue is that at most crop sites with available observations, crop rotation is widely used (especially wheat and maize rotation), an agricultural management practice which is currently not simulated in CLM. In the future, with a CLM module simulating crop rotation, the performance of

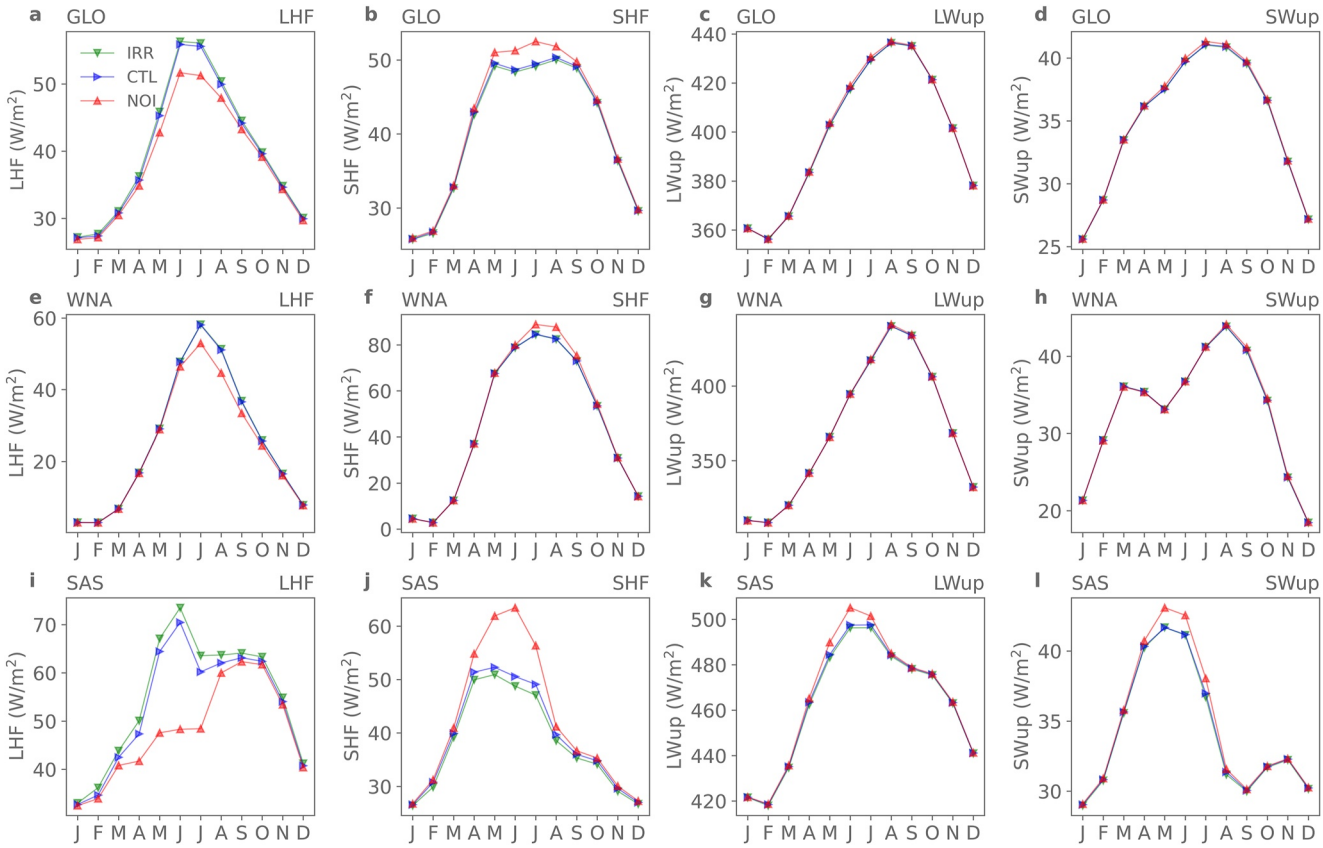

Figure 11. Multi-year average monthly simulated latent heat flux, sensible heat flux, upwelling longwave radiation and upwelling shortwave radiation over global (GLO; a–d), Western North America (WNA: e–h) and South Asia (SAS: i–l) irrigated land. The analysis period is 1986–2015.

water and energy cycle simulations over croplands could be further improved. Second, the irrigation distribution map data contains uncertainties. The gridded data was generated by a decision tree approach, as the statistical data of irrigation methods are only available at the national scale (FAO, 2014; Jägermeyr et al., 2015). As mentioned in Section 2.4, we further simplify the irrigation method distribution map to reduce CLM computation time. In the future, if computation allows, simulations with a more realistic irrigation method distribution map could be conducted, which may help to further improve the model. Third, in all simulations of this study we do not consider the atmosphere-land, ocean-land and atmosphere-ocean interactions, as we conduct land-only simulations to evaluate the impact of the new irrigation module. However, irrigation has been shown to change local and non-local meteorological conditions (e.g., Chen & Jeong, 2018; Chou et al., 2018; de Vrese et al., 2016). Ignoring these effects may be a reason for the neutral performance of the new module in single-point simulations, thus in future studies, coupled simulations of CESM should be conducted to detect the irrigation-induced impacts on climate. Finally, in our global simulations, we use the crop model of CLM, which controls crop phenology based on series of meteorological conditions, but in reality, the crop calendar is more affected by farmers' decisions. In future, if allowed by CLM, global simulations with satellite phenology for different CFTs may be better for these studies.

More developments could still be made to further improve the performance of the model. First, in our development, some values, such as target and threshold soil water, are kept adjustable. A calibration of these parameters could potentially further improve the ability of the model to reproduce global irrigation water withdrawal. Second, we do not account for conveyance and application losses, which may be the reason for the underestimations of irrigation water withdrawal over some regions, and implementing irrigation water use efficiency could further improve the model performance over these regions. At the same time, with some newly developed irrigation techniques in this study, soil moisture cannot be kept at the design level (Figure A1b,A1c), which may cause yield penalties. To solve this problem, calibration of the quantity of extra water used for irrigation could be

done in future studies. Third, in our simulations the limitation of water availability is not applied, as the irrigation water sources are not always well represented in CLM. This may be the reason for the overestimation over some regions. As our simulations do not impose water availability limitations, the irrigation-induced impacts in this study should be considered as potential impacts. A better representation of various water sources and limitations of irrigation water will be needed if we want to further optimize the simulation of irrigation water quantity and simulate the irrigation-induced effects more realistically in CLM. Moreover, some specific irrigation methods may need further developments. In this study, for cropland irrigated by drip irrigation, we use the original scheme, which entails some limitations. Although the irrigation amount is calculated as the deficit between target soil water and actual soil water, runoff and evaporation losses may occur during irrigation application, as water is applied to the soil surface. To avoid this problem, in the LPJmL model, developers apply drip irrigation under surface, and decreased the soil evaporation of irrigation water by 60% (Jägermeyr et al., 2015). In ORCHIDEE, the amount of water used for drip irrigation is assigned as the deficit between potential TR and precipitation plus reinfiltration (Yin, Wang, et al., 2020). In our study, drip irrigation is the dominant method in only a very limited number of grid cells worldwide, hence we did not further modify this scheme. However, when analyzing the effects of drip irrigation method, further improvements of this irrigation technique may be useful. At the same time, for paddy irrigation, the activation condition is based on soil moisture deficit, but in reality, farmers also apply irrigation for other reasons like pest control. Furthermore, for all irrigation methods, the water is not uniformly applied in reality. For example, in drip irrigation water is applied at the root zone of crop plants, and in sprinkler irrigation water is sprayed in a circle, rather than uniformly applied over the whole field. To solve this problem, an additional parameter, distribution uniformity, was introduced and used by Burt et al. (1997) and Jägermeyr et al. (2015). However, in the current CLM representation, it is not straightforward to implement this distribution uniformity functionality, as water is automatically applied over the whole cropland for each CFT.

5. Conclusion

In this study we implement various irrigation methods in the CLM. These irrigation methods vary in the amount of water used for irrigation, method of application and ability to store the surface water. Based on our evaluation of irrigation water withdrawal, we find an optimal combination of irrigation techniques (surface, sprinkler and paddy_3), and implement it as the new irrigation module. Then, by conducting single-point simulations, we detect the impacts of irrigation on evapotranspiration components and surface energy fluxes. Finally, we employ the new irrigation module to detect the irrigation-induced impacts on global water cycle and energy balance. Results reveal that the impacts of different irrigation methods on surface water and energy budgets vary by region, season, and irrigation method, affecting the magnitude and pattern of global irrigation-induced impacts. It indicates that considering the spatial heterogeneity of irrigation methods is important for analyzing the impacts of irrigation on climate. Our newly developed irrigation module substantially improves the ability to simulate irrigation water withdrawals and considers different irrigation techniques, making it a useful tool to study these impacts.

Appendix A

In Table A1 the corresponding Crop Function Types (CFTs) in the data from Jägermeyr et al. (2015) and the CLM surface dataset are shown. There are 14 CFTs in the data from Jägermeyr et al. (2015) and 32 irrigated CFTs in the CLM surface dataset (one is not included in the table as it indicates the general irrigated crop). The meteorological variables used for forcing the model are listed in Table A2, and the difference between the settings of global and single-point simulations are listed in Table A3.

Table A1
Corresponding Crop Functional Types (CFTs) in Data and in Community Land Model (CLM)

CFTs in Jägermeyr et al. (2015)	CFTs in CLM
Temperate cereals	Spring wheat
	Winter wheat
	Barley
	Winter barley
	Rye
	Winter rye
Rice	Rice
Maize	Temperate maize
	Tropical maize
Tropical cereals	Millet
	Sorghum
Pulses	Pulses
Temperate roots	Sugar beet
Tropical roots	Cassava
Sunflower	Sunflower
Soybean	Temperate soybean
	Tropical soybean
Groundnut	Groundnuts
Rapeseed	Rapeseed
Sugarcane	Sugarcane
Others	Citrus
	Cocoa
	Coffee
	Cotton
	Date palm
	Grapes
	Oil palm
	Potatoes
Managed grasslands	Fodder grass
	Miscanthus
	Switchgrass

Table A2
Meteorological Variables in Forcing Data

Variable	Long name	Unit
TBOT	Temperature at the lowest atmosphere level	K
PRECTmms	Total precipitation	mm H_2O/s
FSDS	Total incident solar radiation	W/m^2
FLDS	Incident longwave radiation	W/m^2
PSRF	Surface pressure at the lowest atmosphere level	Pa
WIND	Wind speed at the lowest atmosphere level	m/s
QBOT (RH)[a]	Specific (relative) humidity at the lowest atmosphere level	kg/kg (%)

[a]Only one of these two variables is required.

Table A3
Settings of Global and Single-Point Simulations

Simulations	CFTs	Vegetation state	Crop model	Water availability limitation
Global	Multi	Prognostic	On	No
Single-point	Single	Prescribed	Off	No

Figure A1 shows the simulated daily root zone (0-0.6 m) soil moisture of three simulations and monthly LAI in the three sites (Nebraska, Castellaro and Mase). In all three sites, turning on irrigation (CTL-NOI or IRR-NOI) can substantially alleviate the water stress in all three sites. However, the differences between the original and the new irrigation module (IRR-CTL) vary. The differences are related to the irrigation technique applied (sprinkler in NEB, flood in CAS and paddy_3 in MAS). Figure A2 provides the observed downwelling longwave radiation (LWdown) and downwelling shortwave radiation (SWdown) which are used to force the single-point simulations, and simulated ground heat flux (GHF) and net radiation (Rnet) for different simulations over all three sites. Figure A3, A4, A5, and A6 show the differences in hydrological and energy variables between the simulation with the old irrigation module and the simulation without irrigation (CTL-NOI) and between the simulations with the original and the new irrigation modules (IRR-CTL). Figure A7 and A8 provide the multi-year average monthly simulated hydrological and energy variables for other three regions (MED, EAS and ESA).

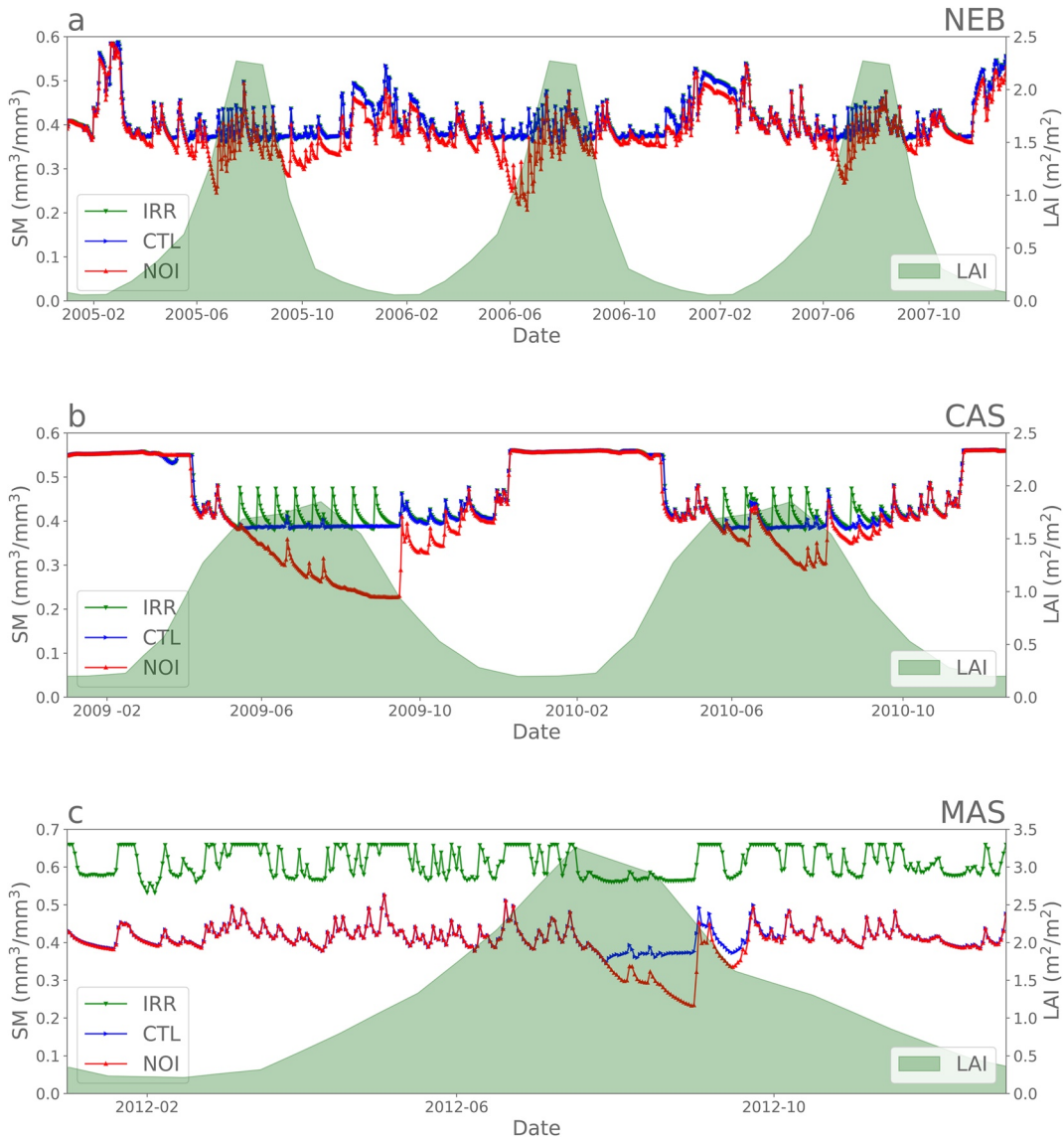

Figure A1. Daily simulated root zone (0–0.6 m) soil moisture (SM) and observed land area index (LAI) in Nebraska (NEB: 2005–2007), Castellaro (CAS: 2009–2010) and Mase (2012). The LAI data used here is a monthly LAI climatology from MODIS.

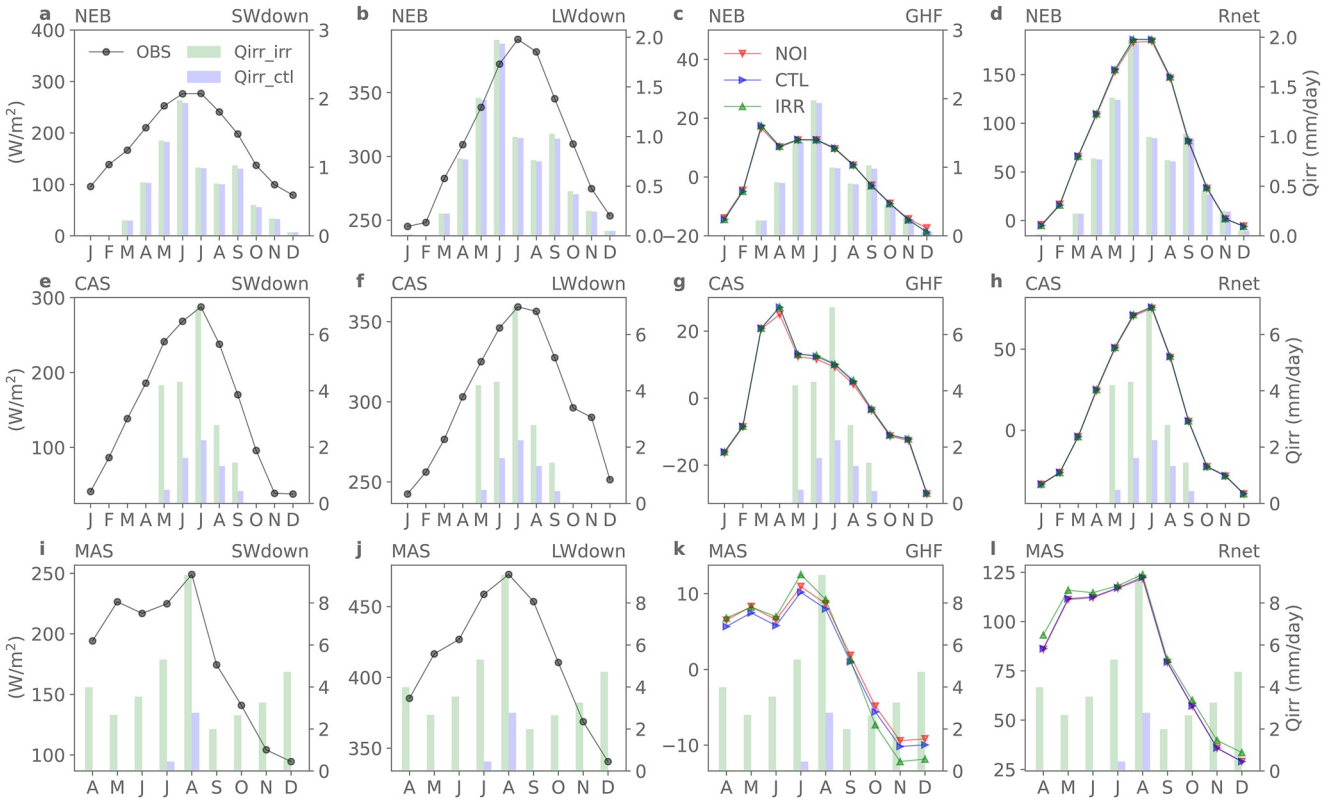

Figure A2. Multi-year average monthly observed downwelling longwave radiation (LWdown), downwelling shortwave radiation (SWdown) (black line) and simulated ground heat flux (GHF) and net radiation (Rnet) of NOI (red lines), CTL (blue lines) and IRR (green lines), and simulated irrigation water amount of CTL (blue bars) and IRR (green bars) in Nebraska (NEB), Castellaro (CAS) and Mase (MAS). The simulation periods can be found in Table 4.

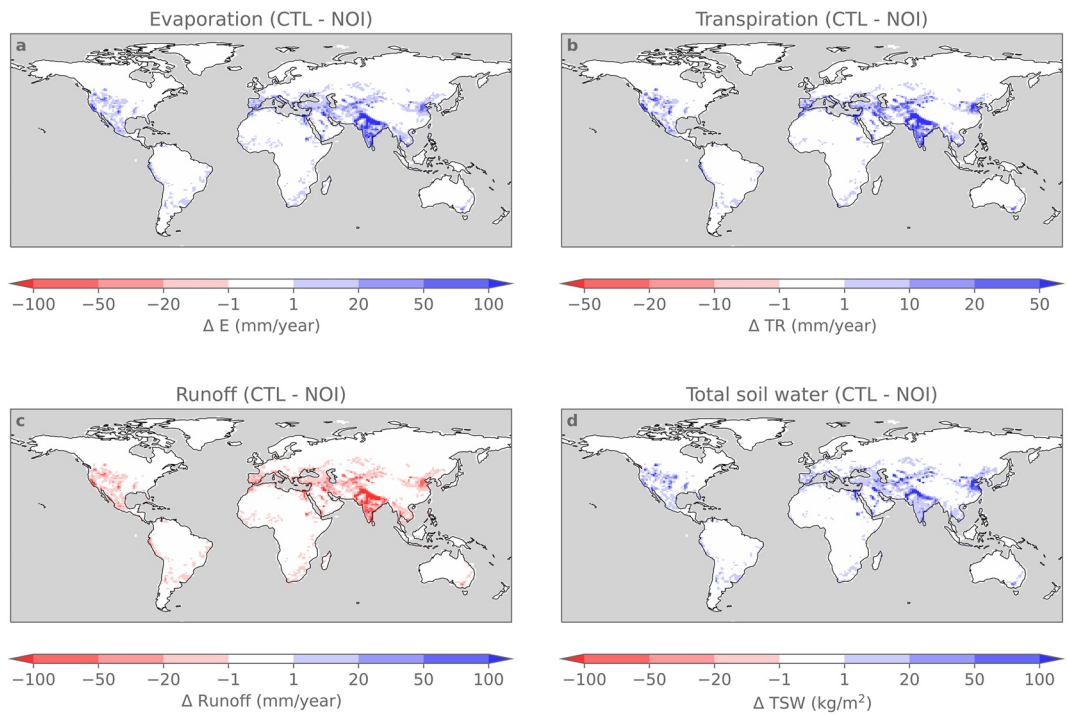

Figure A3. Impacts of irrigation with the original irrigation module (CTL-NOI) on the water cycle, including evaporation (a), transpiration (b), runoff (c) and total column soil water (d).

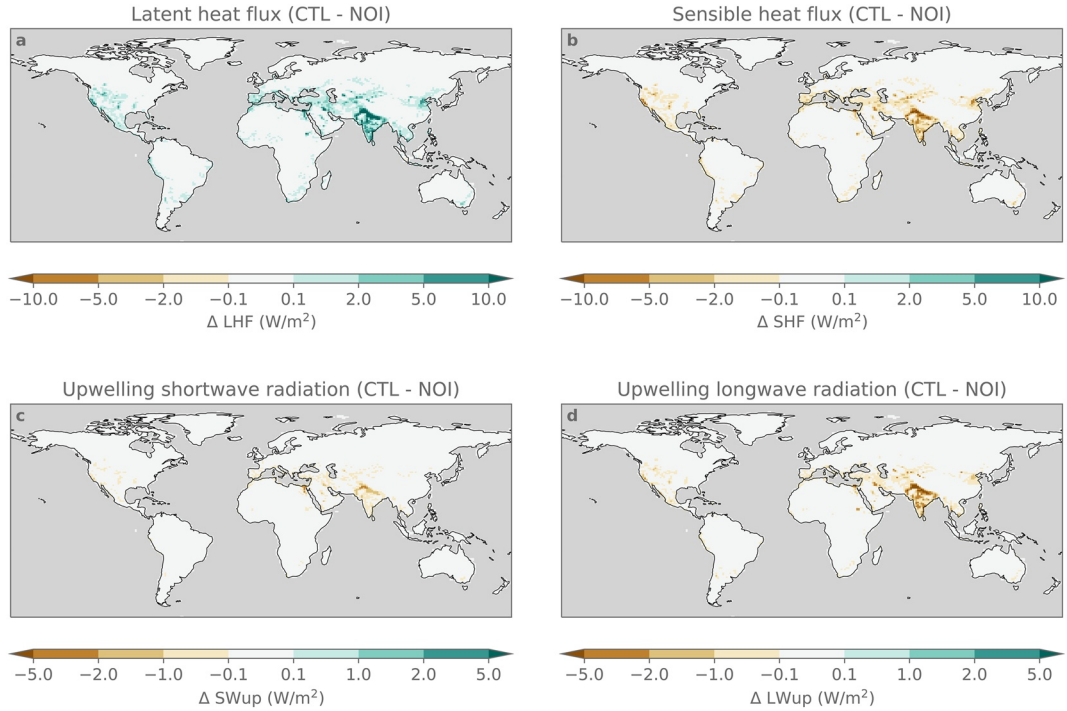

Figure A4. Impacts of irrigation with the original irrigation module (CTL-NOI) on the energy cycle, including latent heat flux (a), sensible heat flux (b), upwelling shortwave radiation (c) and upwelling longwave radiation (d).

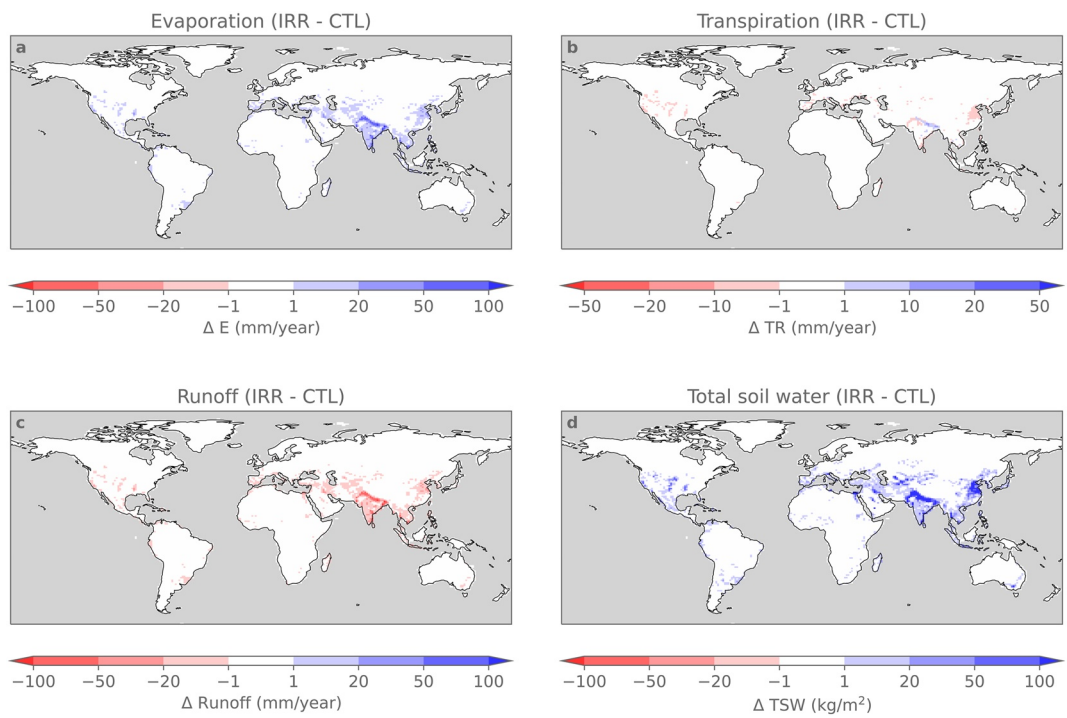

Figure A5. Difference between the impacts of irrigation with two irrigation modules (IRR-NOI) on the water cycle, including evaporation (a), transpiration (b), runoff (c) and total column soil water (d).

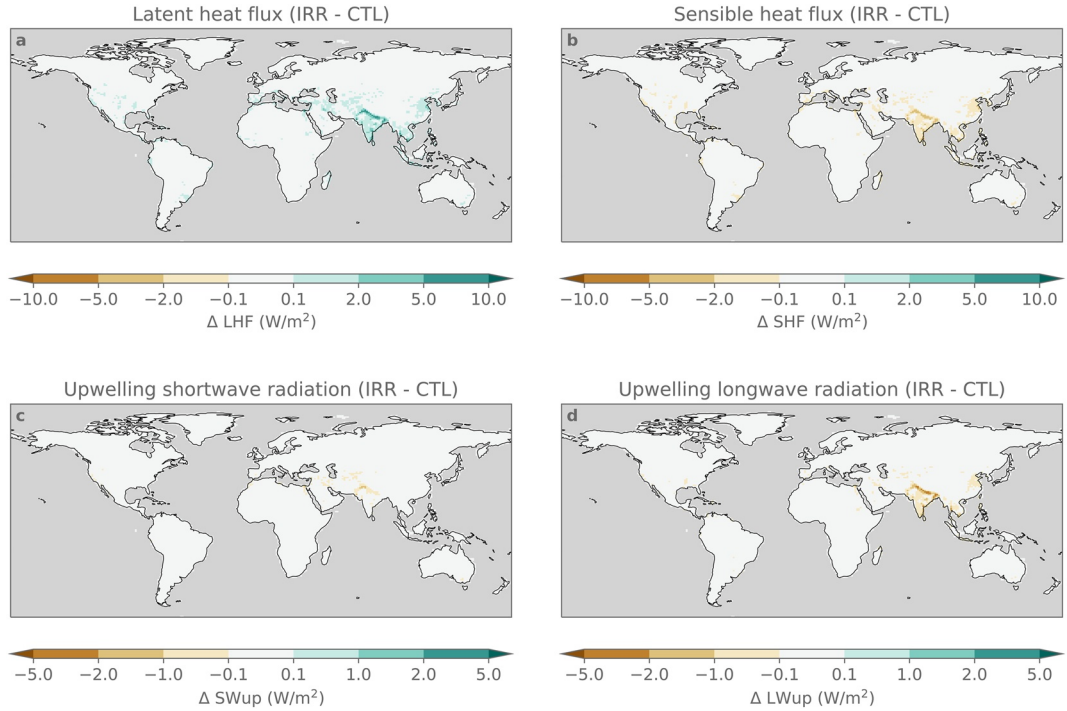

Figure A6. Difference between the impacts of irrigation with two irrigation modules (IRR-NOI) on the water cycle, including evaporation (a), transpiration (b), runoff (c) and total column soil water (d).

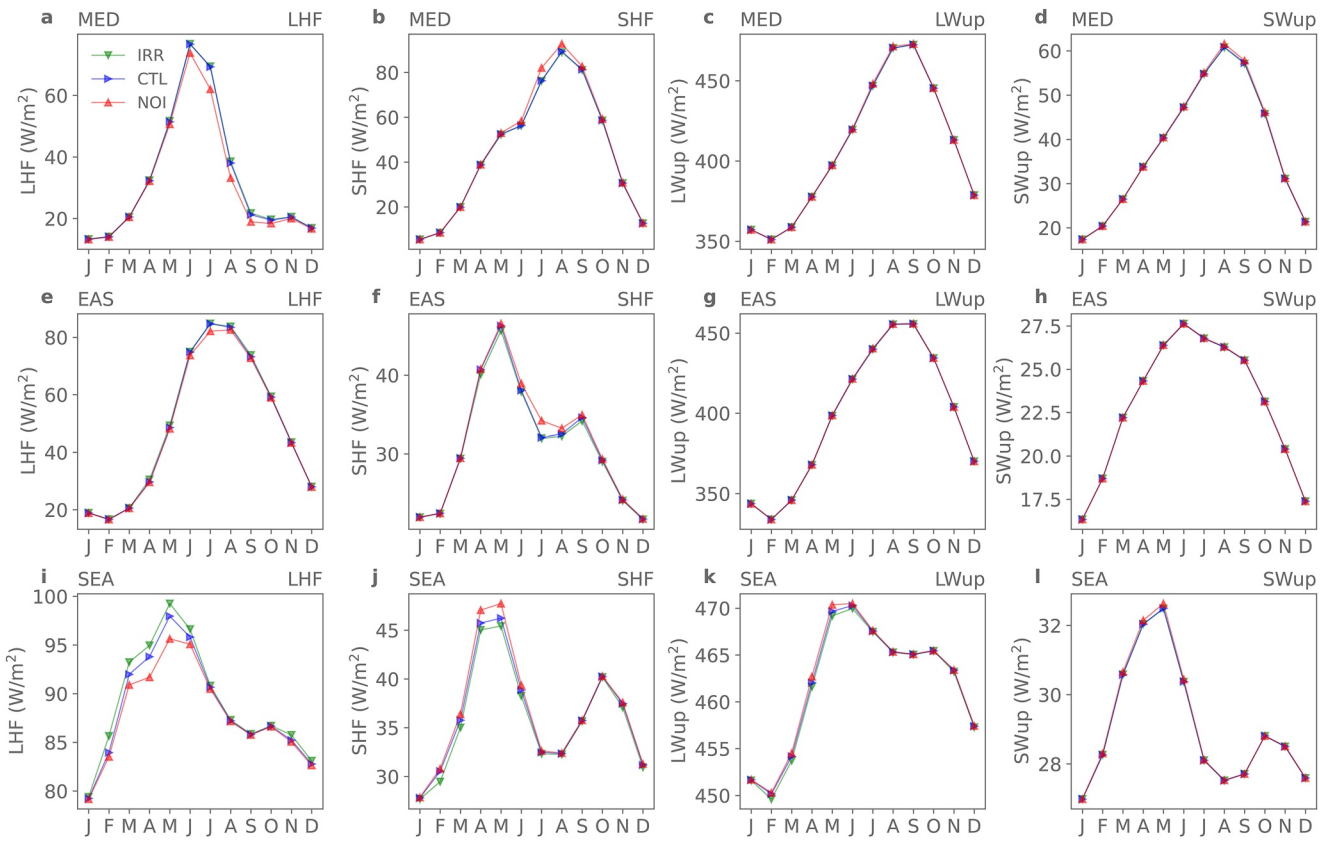

Figure A7. Multi-year average monthly simulated evaporation, transpiration, runoff and total water storage over Mediterranean (MED: a–d), East Asia (EAS: e–h), Southeast Asia (SEA: i–l) irrigated land. The analysis period is 1986–2015.

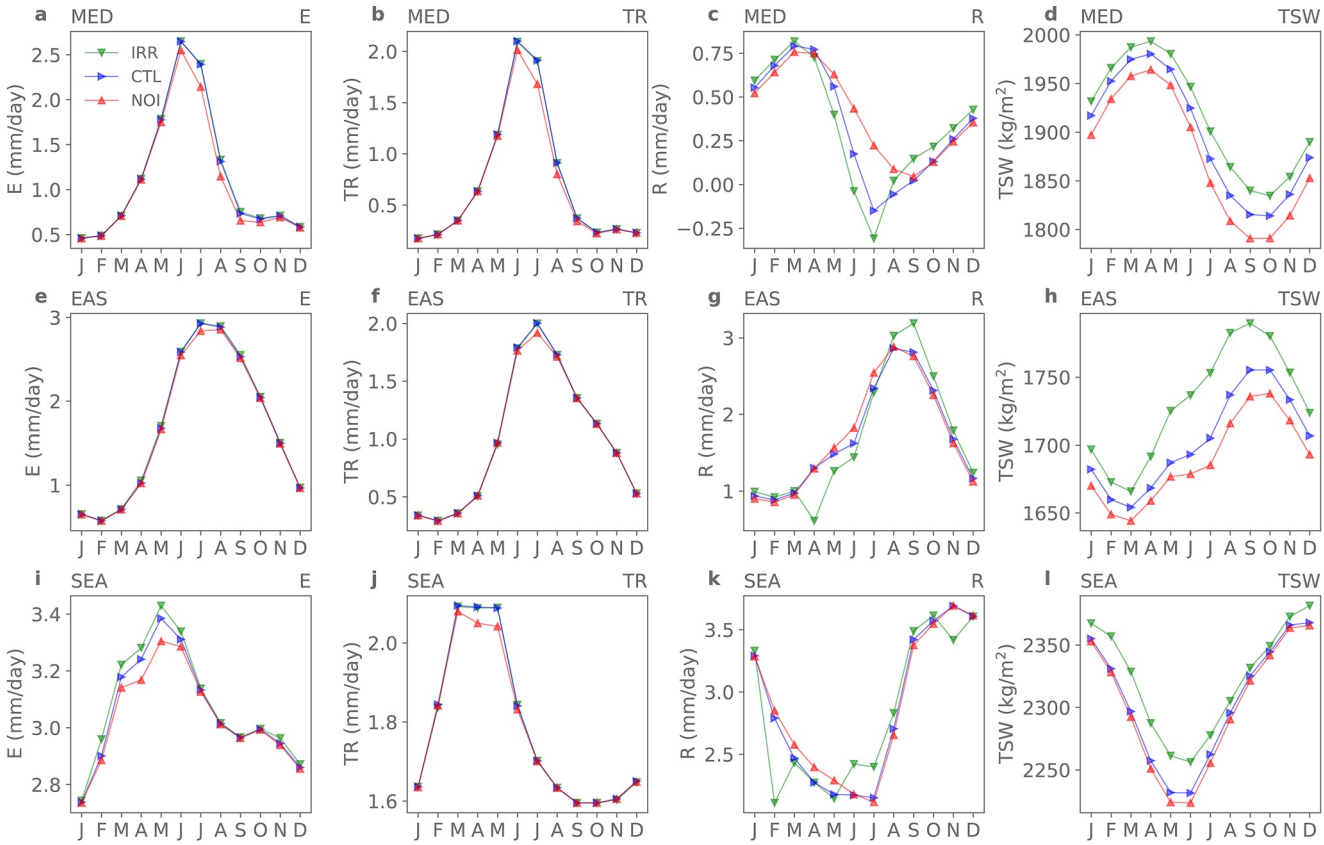

Figure A8. Multi-year average monthly simulated latent heat flux, sensible heat flux, upwelling longwave radiation and upwelling shortwave radiation over Mediterranean (MED: a–d), East Asia (EAS: e–h), Southeast Asia (SEA: i–l) irrigated land. The analysis period is 1986–2015.

Data Availability Statement

CLM5 is publicly available through the Community Terrestrial System Model (CTSM) repository: https://github.com/ESCOMP/CTSM/. All scripts developed for this study are available at: https://github.com/VUB-HYDR/2022_Yao_etal_JAMES/tree/0.1.0; https://doi.org/10.5281/zenodo.7104997. Finally, all data used in simulations and analysis are available at https://doi.org/10.6084/m9.figshare.20711392.v1.

Acknowledgments
We would like to thank two anonymous reviewers and the editor for their constructive suggestions and comments. We also want to thank Bill Sacks for helpful suggestions about irrigation module development. Y.Y. holds a China Scholarship Council (CSC) Studentship with Vrije Universiteit Brussel. I.V. is a research fellow at the Research Foundation Flanders (FWO) (FWOTM920). The computational resources and services used in this work were provided by the VSC (Flemish Supercomputer Center), funded by the Research Foundation—Flanders (FWO) and the Flemish Government—department EWI. This study was supported by the LAMACLIMA project, part of AXIS, an ERA-NET initiated by JPI Climate, and funded by BELSPO (BE, Grant B2/181/P1) with co-funding by the European Union (Grant 776608). J.J. was supported by the NASA GISS Climate Impacts Group and the Open Philanthropy Project.

References

Bouman, B. (2007). *Water management in irrigated rice: Coping with water scarcity*. International Rice Research Institute.

Burt, C. M., Clemmens, A. J., Strelkoff, T. S., Solomon, K. H., Bliesner, R. D., Hardy, L. A., et al. (1997). Irrigation performance measures: Efficiency and uniformity. *Journal of Irrigation and Drainage Engineering*, *123*(6), 423–442. https://doi.org/10.1061/(asce)0733-9437(1997)123:6(423)

Chen, X., & Jeong, S.-J. (2018). Irrigation enhances local warming with greater nocturnal warming effects than daytime cooling effects. *Environmental Research Letters*, *13*(2), 024005. https://doi.org/10.1088/1748-9326/aa9dea

Cheng, Y., Huang, M., Zhu, B., Bisht, G., Zhou, T., Liu, Y., et al. (2021). Validation of the community land model version 5 over the contiguous United States (CONUS) using in situ and remote sensing data sets. *Journal of Geophysical Research: Atmospheres*, *126*(5), e2020JD033539. https://doi.org/10.1029/2020jd033539

Chou, C., Ryu, D., Lo, M.-H., Wey, H.-W., & Malano, H. M. (2018). Irrigation-induced land–atmosphere feedbacks and their impacts on Indian summer monsoon. *Journal of Climate*, *31*(21), 8785–8801. https://doi.org/10.1175/jcli-d-17-0762.1

Cook, B. I., Puma, M. J., & Krakauer, N. Y. (2011). Irrigation induced surface cooling in the context of modern and increased greenhouse gas forcing. *Climate Dynamics*, *37*(7), 1587–1600. https://doi.org/10.1007/s00382-010-0932-x

Cook, B. I., Shukla, S. P., Puma, M. J., & Nazarenko, L. S. (2015). Irrigation as an historical climate forcing. *Climate Dynamics*, *44*(5–6), 1715–1730. https://doi.org/10.1007/s00382-014-2204-7

Danabasoglu, G., Lamarque, J.-F., Bacmeister, J., Bailey, D., DuVivier, A., Edwards, J., et al. (2020). The community earth system model version 2 (CESM2). *Journal of Advances in Modeling Earth Systems*, *12*(2), e2019MS001916. https://doi.org/10.1029/2019ms001916

Devanand, A., Huang, M., Ashfaq, M., Barik, B., & Ghosh, S. (2019). Choice of irrigation water management practice affects Indian summer monsoon rainfall and its extremes. *Geophysical Research Letters*, *46*(15), 9126–9135. https://doi.org/10.1029/2019gl083875

de Vrese, P., Hagemann, S., & Claussen, M. (2016). Asian irrigation, African rain: Remote impacts of irrigation. *Geophysical Research Letters*, *43*(8), 3737–3745. https://doi.org/10.1002/2016gl068146

Döll, P., Fiedler, K., & Zhang, J. (2009). Global-scale analysis of river flow alterations due to water withdrawals and reservoirs. *Hydrology and Earth System Sciences*, *13*(12), 2413–2432. https://doi.org/10.5194/hess-13-2413-2009

FAO. (2014). AQUASTAT Database, Food and Agriculture Organization of the United Nations (FAO). Retrieved from http://www.fao.org/nr/water/aquastat/data/query/index.html?lang=en

Ferguson, I. M., & Maxwell, R. M. (2012). Human impacts on terrestrial hydrology: Climate change versus pumping and irrigation. *Environmental Research Letters*, *7*(4), 044022. https://doi.org/10.1088/1748-9326/7/4/044022

Fisher, R. A., Wieder, W. R., Sanderson, B. M., Koven, C. D., Oleson, K. W., Xu, C., et al. (2019). Parametric controls on vegetation responses to biogeochemical forcing in the CLM5. *Journal of Advances in Modeling Earth Systems*, *11*(9), 2879–2895. https://doi.org/10.1029/2019ms001609

Guimberteau, M., Laval, K., Perrier, A., & Polcher, J. (2012). Global effect of irrigation and its impact on the onset of the Indian summer monsoon. *Climate Dynamics*, *39*(6), 1329–1348. https://doi.org/10.1007/s00382-011-1252-5

Hanasaki, N., Kanae, S., Oki, T., Masuda, K., Motoya, K., Shirakawa, N., et al. (2008). An integrated model for the assessment of global water resources—Part 2: Applications and assessments. *Hydrology and Earth System Sciences*, *12*(4), 1027–1037. https://doi.org/10.5194/hess-12-1027-2008

Hao, Z., Chen, S., Li, Z., Yu, Z., Shao, Q., Yuan, F., & Shi, F. (2015). Quantitative assessment of the impacts of irrigation on surface water fluxes in the Tarim River, China. *Hydrology Research*, *46*(6), 996–1007. https://doi.org/10.2166/nh.2015.215

Harding, K. J., & Snyder, P. K. (2012). Modeling the atmospheric response to irrigation in the Great Plains. Part I: General impacts on precipitation and the energy budget. *Journal of Hydrometeorology*, *13*(6), 1667–1686. https://doi.org/10.1175/jhm-d-11-098.1

Hauser, M., Thiery, W., & Seneviratne, S. I. (2019). Potential of global land water recycling to mitigate local temperature extremes. *Earth System Dynamics*, *10*(1), 157–169. https://doi.org/10.5194/esd-10-157-2019

Hirsch, A. L., Prestele, R., Davin, E. L., Seneviratne, S. I., Thiery, W., & Verburg, P. H. (2018). Modelled biophysical impacts of conservation agriculture on local climates. *Global Change Biology*, *24*(10), 4758–4774. https://doi.org/10.1111/gcb.14362

Hirsch, A. L., Wilhelm, M., Davin, E. L., Thiery, W., & Seneviratne, S. I. (2017). Can climate-effective land management reduce regional warming? *Journal of Geophysical Research: Atmospheres*, *122*(4), 2269–2288. https://doi.org/10.1002/2016jd026125

Iturbide, M., Gutiérrez, J. M., Alves, L. M., Bedia, J., Cerezo-Mota, R., Cimadevilla, E., et al. (2020). An update of IPCC climate reference regions for subcontinental analysis of climate model data: Definition and aggregated datasets. *Earth System Science Data*, *12*(4), 2959–2970. https://doi.org/10.5194/essd-12-2959-2020

Iwata, H. (2012). FLUXNET-CH4 JP-MSE Mase rice paddy field [Dataset]. FLUXNET-CH4 Community Product. https://doi.org/10.18140/FLX/1669647

Jägermeyr, J., Gerten, D., Heinke, J., Schaphoff, S., Kummu, M., & Lucht, W. (2015). Water savings potentials of irrigation systems: Global simulation of processes and linkages. *Hydrology and Earth System Sciences*, *19*(7), 3073–3091. https://doi.org/10.5194/hess-19-3073-2015

Kueppers, L. M., Snyder, M. A., & Sloan, L. C. (2007). Irrigation cooling effect: Regional climate forcing by land-use change. *Geophysical Research Letters*, *34*(3), L03703. https://doi.org/10.1029/2006gl028679

Lawrence, D., Fisher, R., Koven, C., Oleson, K., Swenson, S., Bonan, G., et al. (2019). The community land model version 5: Description of new features, benchmarking, and impact of forcing uncertainty. *Journal of Advances in Modeling Earth Systems*, *11*(12), 4245–4287. https://doi.org/10.1029/2018ms001583

Lawrence, D., Rosie, F., Koven, C., Oleson, K., Swenson, S., Vertenstein, M., et al. (2018). CLM5.0 technical description (computer software manual).

Leng, G., Huang, M., Tang, Q., Gao, H., & Leung, L. R. (2014). Modeling the effects of groundwater-fed irrigation on terrestrial hydrology over the conterminous United States. *Journal of Hydrometeorology*, *15*(3), 957–972. https://doi.org/10.1175/jhm-d-13-049.1

Leng, G., Huang, M., Tang, Q., & Leung, L. R. (2015). A modeling study of irrigation effects on global surface water and groundwater resources under a changing climate. *Journal of Advances in Modeling Earth Systems*, *7*(3), 1285–1304. https://doi.org/10.1002/2015ms000437

Leng, G., Leung, L. R., & Huang, M. (2017). Significant impacts of irrigation water sources and methods on modeling irrigation effects in the acme land model. *Journal of Advances in Modeling Earth Systems*, *9*(3), 1665–1683. https://doi.org/10.1002/2016ms000885

Lombardozzi, D. L., Lu, Y., Lawrence, P. J., Lawrence, D. M., Swenson, S., Oleson, K. W., et al. (2020). Simulating agriculture in the community land model version 5. *Journal of Geophysical Research: Biogeosciences*, *125*(8), e2019JG005529. https://doi.org/10.1029/2019jg005529

Manca, G., & Goded, I. (2009–2010). FLUXNET-CH4 IT-CAS Castellaro [Dataset]. FLUXNET-CH4 Community Product. https://doi.org/10.18140/FLX/1669645

McGuire, V. L. (2014). Water-level changes and change in water in storage in the high plains aquifer, predevelopment to 2013 and 2011–13.

Meier, J., Zabel, F., & Mauser, W. (2018). A global approach to estimate irrigated areas—A comparison between different data and statistics. *Hydrology and Earth System Sciences*, *22*(2), 1119–1133. https://doi.org/10.5194/hess-22-1119-2018

Meier, R., Davin, E. L., Swenson, S. C., Lawrence, D. M., & Schwaab, J. (2019). Biomass heat storage dampens diurnal temperature variations in forests. *Environmental Research Letters*, *14*(8), 084026. https://doi.org/10.1088/1748-9326/ab2b4e

Nocco, M. A., Smail, R. A., & Kucharik, C. J. (2019). Observation of irrigation-induced climate change in the Midwest United States. *Global Change Biology*, *25*(10), 3472–3484. https://doi.org/10.1111/gcb.14725

Ozdogan, M., Rodell, M., Beaudoing, H. K., & Toll, D. L. (2010). Simulating the effects of irrigation over the United States in a land surface model based on satellite-derived agricultural data. *Journal of Hydrometeorology*, *11*(1), 171–184. https://doi.org/10.1175/2009jhm1116.1

Portmann, F. T., Siebert, S., & Döll, P. (2010). Mirca2000—Global monthly irrigated and rainfed crop areas around the year 2000: A new high-resolution data set for agricultural and hydrological modeling. *Global Biogeochemical Cycles*, *24*(1), GB1011. https://doi.org/10.1029/2008gb003435

Puma, M., & Cook, B. (2010). Effects of irrigation on global climate during the 20th century. *Journal of Geophysical Research*, *115*(D16), D16120. https://doi.org/10.1029/2010jd014122

Sacks, W. J., Cook, B. I., Buenning, N., Levis, S., & Helkowski, J. H. (2009). Effects of global irrigation on the near-surface climate. *Climate Dynamics*, *33*(2), 159–175. https://doi.org/10.1007/s00382-008-0445-z

Saeed, F., Hagemann, S., & Jacob, D. (2009). Impact of irrigation on the south Asian summer monsoon. *Geophysical Research Letters*, *36*(20), L20711. https://doi.org/10.1029/2009gl040625

Schultz, B., Thatte, C., & Labhsetwar, V. (2005). Irrigation and drainage. Main contributors to global food production. *Irrigation and Drainage: The journal of the International Commission on Irrigation and Drainage*, *54*(3), 263–278. https://doi.org/10.1002/ird.170

Siebert, S., Kummu, M., Porkka, M., Döll, P., Ramankutty, N., & Scanlon, B. (2015). A global dataset of the extent of irrigated land from 1900 to 2005. *Hydrology and Earth System Sciences*, *19*, 1521–1545. https://doi.org/10.5194/hess-19-1521-2015

Suyker, A. (2001–2013). FLUXNET2015 US-Ne1 Mead—Irrigated continuous maize site [Dataset]. US-Ne2. https://doi.org/10.18140/FLX/1440084

Telteu, C.-E., Müller Schmied, H., Thiery, W., Leng, G., Burek, P., Liu, X., et al. (2021). Understanding each other's models: An introduction and a standard representation of 16 global water models to support intercomparison, improvement, and communication. *Geoscientific Model Development*, *14*(6), 3843–3878. https://doi.org/10.5194/gmd-14-3843-2021

Thiery, W., Davin, E. L., Lawrence, D. M., Hirsch, A. L., Hauser, M., & Seneviratne, S. I. (2017). Present-day irrigation mitigates heat extremes. *Journal of Geophysical Research: Atmospheres*, *122*(3), 1403–1422. https://doi.org/10.1002/2016jd025740

Thiery, W., Visser, A. J., Fischer, E. M., Hauser, M., Hirsch, A. L., Lawrence, D. M., et al. (2020). Warming of hot extremes alleviated by expanding irrigation. *Nature Communications*, *11*(1), 1–7. https://doi.org/10.1038/s41467-019-14075-4

Valmassoi, A., Dudhia, J., Sabatino, S. D., & Pilla, F. (2020). Evaluation of three new surface irrigation parameterizations in the WRF-ARW v3. 8.1 model: The Po Valley (Italy) case study. *Geoscientific Model Development*, *13*(7), 3179–3201. https://doi.org/10.5194/gmd-13-3179-2020

Vanderkelen, I., Gharari, S., Mizukami, N., Clark, M. P., Lawrence, D. M., Swenson, S., et al. (2022). Evaluating a reservoir parametrisation in the vector-based global routing model mizuRoute (v2. 0.1) for Earth system model coupling. *Geoscientific Model Development Discussions*, *15*(10), 1–41. https://doi.org/10.5194/gmd-15-4163-2022

Van der Kooij, S., Zwarteveen, M., Boesveld, H., & Kuper, M. (2013). The efficiency of drip irrigation unpacked. *Agricultural Water Management*, *123*, 103–110. https://doi.org/10.1016/j.agwat.2013.03.014

Wang, J., Jiang, Y., Wang, H., Huang, Q., & Deng, H. (2019). *Groundwater irrigation and management in northern China: Status, trends, and challenges*. International Journal of Water Resources Development. https://doi.org/10.1080/07900627.2019.1584094

Wine, M. L., & Laronne, J. B. (2020). In water-limited landscapes, an Anthropocene exchange: Trading lakes for irrigated agriculture. *Earth's Future*, *8*(4), e2019EF001274. https://doi.org/10.1029/2019ef001274

Wisser, D., Fekete, B. M., Vörösmarty, C., & Schumann, A. (2010). Reconstructing 20th century global hydrography: A contribution to the Global Terrestrial Network-Hydrology (GTN-H). *Hydrology and Earth System Sciences*, *14*(1), 1–24. https://doi.org/10.5194/hess-14-1-2010

WWAP. (2019). Leaving no one behind (technical report).

Yin, L., Xu, Z., Liu, M., Xu, T., Wang, T., Liao, W., et al. (2020). Estimation of biogenic volatile organic compound (BVOC) emissions in China using WRF–CLM–MEGAN coupled model. *Biogeosciences Discussions*, 1–30. https://doi.org/10.5194/bg-2019-458

Yin, Z., Wang, X., Ottlé, C., Zhou, F., Guimberteau, M., Polcher, J., et al. (2020). Improvement of the irrigation scheme in the ORCHIDEE land surface model and impacts of irrigation on regional water budgets over China. *Journal of Advances in Modeling Earth Systems*, *12*(4), e2019MS001770. https://doi.org/10.1029/2019ms001770

Zhou, F., Bo, Y., Ciais, P., Dumas, P., Tang, Q., Wang, X., et al. (2020). Deceleration of China's human water use and its key drivers. *Proceedings of the National Academy of Sciences*, *117*(14), 7702–7711. https://doi.org/10.1073/pnas.1909902117

Zhu, B., Huang, M., Cheng, Y., Xie, X., Liu, Y., Zhang, X., et al. (2020). Effects of irrigation on water, carbon, and nitrogen budgets in a semiarid watershed in the Pacific northwest: A modeling study. *Journal of Advances in Modeling Earth Systems*, *12*(9), e2019MS001953. https://doi.org/10.1029/2019ms001953

Zohaib, M., & Choi, M. (2020). Satellite-based global-scale irrigation water use and its contemporary trends. *Science of the Total Environment*, *714*, 136719. https://doi.org/10.1016/j.scitotenv.2020.136719